Research Paper

Lycopene prevents carcinogen-induced cutaneous tumor by enhancing activation of the Nrf2 pathway through p62-triggered autophagic Keap1 degradation

Siliang Wang[1,3,*], Yuan-Yuan Wu[1,*], Xu Wang[1,*], Peiliang Shen[1], Qi Jia[1], Suyun Yu[1], Yuan Wang[1], Xiaoman Li[1], Wenxing Chen[1], Aiyun Wang[1], Yin Lu[1,2]

[1]Jiangsu Key Laboratory for Pharmacology and Safety Evaluation of Chinese Materia Medica, School of Pharmacy, Nanjing University of Chinese Medicine, Nanjing 210023, P.R. China
[2]Jiangsu Collaborative Innovation Center of Traditional Chinese Medicine (TCM) Prevention and Treatment of Tumor, Nanjing University of Chinese Medicine, Nanjing 210023, P.R. China
[3]Nanjing Drum Tower Hospital, The Affiliated Hospital of Nanjing University Medical School, Nanjing 210008, P.R. China
*Equal contribution

Correspondence to: Wenxing Chen, Aiyun Wang, Yin Lu; **email:** chenwx@njucm.edu.cn, wangaiyun@njucm.edu.cn, luyingreen@njucm.edu.cn
Keywords: lycopene, cutaneous tumor, autophagy, Nrf2, chemoprevention
Received: December 21, 2019 **Accepted:** March 30, 2020 **Published:** May 4, 2020

ABSTRACT

Biologically active natural products have been used for the chemoprevention of cutaneous tumors. Lycopene is the main active phytochemical in tomatoes. We herein aimed to assess the cancer preventive effects of lycopene and to find potential molecular targets. In chemically-induced cutaneous tumor mice and cell models, lycopene attenuated cutaneous tumor incidence and multiplicity as well as the tumorigenesis of normal cutaneous cells in phase-selectivity (only in the promotion phase) manners. By utilizing a comprehensive approach combining bioinformatics with network pharmacology, we predicted that intracellular autophagy and redox status were associated with lycopene's preventive effect on cutaneous tumors. Lycopene stimulated the activation of antioxidant enzymes and the translocation of the transcription factor Nrf2 (nuclear factor erythroid 2-related factor 2) that predominantly maintained intracellular redox equilibrium. The cancer chemopreventive effects were mediated by Nrf2. Further, lycopene enhanced the expression of autophagy protein p62. Therefore this led to the degradation of Keap1(Kelch ECH associating protein 1), the main protein locking Nrf2 in cytoplasm. In conclusion, our study provides preclinical evidence of the chemopreventive effects of lycopene on cutaneous tumors and reveals the mechanistic link between lycopene's stimulation of Nrf2 signaling pathway and p62-mediated degradation of Keap1 via the autophagy-lysosomal pathway.

INTRODUCTION

As one of the most common cancers worldwide, cutaneous carcinoma has over one million new cases each year, with annual cost for treatment surpassing 8 billion dollars [1, 2]. Nevertheless, it still cannot be effectively treated in regards to both poor clinical outcomes and out-of-pocket expenditure [3, 4]. In an economical, non-toxic, and easily available manner, cancer chemoprevention uses substances to decelerate or to eliminate the progression of intraepithelial precancerous or neoplastic lesions to tumors. Therefore,

cancer chemoprevention therapy has potential economic interests for cutaneous carcinoma and other types with skyrocketing morbidity [5, 6].

Epidemiological evidence supports an association between tomato consumption and reduced risk of prostate cancer. Clinical data suggests that continued consumption of tomato paste can alleviate UV-induced sunburn in humans. Lycopene, the primary phytochemical in tomatoes, has been reported to reduce the risks of many diseases [7, 8], with well-demonstrated anti-inflammatory, antimicrobial, and anti-aging activities [9, 10]. However, the preventive effects of this compound applied topically and the underlying mechanisms remain unclear. To this end, we herein utilized two models of chemically induced tumorigenesis to evaluate the chemopreventive effects of lycopene in vivo and in vitro.

Aggravated redox imbalance may originate from a series of carcinogens and lead to genetic mutation, genomic instability, and neoplastic transformation [11, 12]. The skin is the largest organ enduring external harmful substances, and is thus prone to carcinogenesis. Generally, by inducing sophisticated anti-stress defense responses, normal cutaneous cells adapt to adverse conditions in response to emergencies such as detrimental stress [13, 14]. Carcinogen-induced over-consumption or dysregulation of these processes is related with the pathogenesis of human cancers [15–17]. Therefore, we focused on lycopene-evoked defense mechanism to combat the carcinogens, which might clue the mechanisms that mediate the action of this compound.

Of the main mechanisms for cellular defense against electrophilic and oxidative stresses, the Keap1-Nrf2 system plays a paramount role in preventing cutaneous carcinoma and many other types [18, 19]. On this basis, we used Nrf2-/- mice and Nrf2KD cells to explore the relationship between the preventive effect of lycopene and the Nrf2 signaling pathway and related anti-oxidant system.

Selective autophagy is another important host defense mechanism [20]. Cytoplasmic materials are engulfed by autophagosomes through this bulk-degradation protective system. This system appears constitutively and is induced responding to intracellular stresses to maintain homeostasis by degrading toxic or unnecessary organelles, proteins and, pathogens [21, 22]. p62 protein plays a vital role in selective autophagy, generally acting as a cargo receptor for ubiquitinated substrates that fuse with lysosomes, resulting in substrate degradation [23]. Recently, p62 has been verified to participate in the Nrf2-Keap1 pathway through interacting with the Nrf2-binding site of Keap1 and inhibiting Keap1-Nrf2 interaction competitively, inducing the expressions of gene-encoding antioxidant enzymes [24]. In this study, we identified the endogenous interaction between Keap1 and p62 as well as the degradation of Keap1 in an autophagy-lysosomal manner after treatment with lycopene, which protected Nrf2 from Keap1-induced proteasomal degradation. These findings highlight the significance of lycopene in preventing cutaneous carcinoma, as a skin care supplement, can feasibly reduce the risk of this cancer, through a selective autophagy-controlled Nrf2 pathway activation manner.

RESULTS

Lycopene exerted preventive effects on chemically induced cutaneous tumor only in the promotion phase

A two-stage 7, 12-dimethylbenzanthracene (DMBA)/ 12-O-tetradecanoylphorbol-13-acetate (TPA)-induced model, which has been used in our group and other labs for years as a successful mouse model of cutaneous papilloma, was first employed [17] (Figure 1A). Being organ-specific, it captures well-defined pathological progression from normal tissue to papilloma and finally squamous cell carcinoma (SCC) in human body. This model simulates the multi-step processes (mostly initiation and promotion) of cutaneous carcinogenesis, in which the initiation phase is mediated by DMBA and the promotion phase is induced by TPA [25].

To analyze the roles of lycopene in the two phases, we divided mice into four groups including three treatment groups and one model group with indicated chemical treatment at different stages (Figure 1A). One treatment group (PI group: pretreatment only before initiation) was administered by lycopene before DMBA-mediated initiation until TPA-initiated promotion. Similar to most cancer chemopreventive studies, another treatment group (PP group: pretreatment only before promotion) was administered between initiation and promotion until the end of this study. The third treatment group (PA group: pretreatment in all phases) was administered before DMBA-mediated initiation until the end of this study. With this grouping method, the preventive effects of lycopene on initiation phase, promotion phase and the whole process were assessed respectively.

As shown in Figure 1B, all the DMBA/TPA-treated mice have cutaneous papillomas on dorsal skins. Compared with the model group, pretreatment with lycopene markedly attenuated both the incidence rate (Figure 1C) and multiplicity (Figure 1D) of cutaneous papillomas only in PP and PA groups, and delayed the latency substantially from 5 to 8 weeks. Besides, the

inhibitory effects of lycopene on tumorigenesis were proven by the distribution of papilloma sizes (Figure 1E). Furthermore, the survival rate of the model group plummeted compared with those of PP and PA groups. In the end, only 50% of mice in the model group remained alive, whereas almost all the mice in PP and PA groups survived bearing cutaneous papilloma (Figure 1F). Surprisingly, PP and PA groups had similar cutaneous papilloma incidence rates, multiplicities, latencies, and survival rates, suggesting lycopene exerted evident preventive effects on cutaneous papilloma only in the promotion phase.

Histological analysis further signified that lycopene notably attenuated the increased epidermal thickness (hyperplasia) induced by DMBA/TPA (Figure 1G). Furthermore, basosquamous carcinoma was observed in mouse in model group, and local invasion of basosquamous carcinoma cells can be detected in stroma. However, on the contrary, only the benign papillomas can be found in PA and PP mouse with intact basement membranes and hyperplasia of the overlying epidermis (Figure 1H).

To further demonstrate the preventive effects of lycopene on cutaneous tumors in the promotion phase, we observed the anchorage-independent growth of JB6 P+ cells in soft agar induced by TPA (Figure 2). JB6 P+ cells were pretreated for 5 days with lycopene and then incubated with TPA in the presence or absence of this compound for another 14 days to induce malignant transformation. Pretreatment with 2 or 8 μM lycopene significantly inhibited the colony formation of JB6 P+ cells induced with TPA by about 45% and 71% ($P < 0.001$), respectively. When JB6 P+ cells were incubated in soft agar containing TPA without lycopene for another 14 days, pretreatment with lycopene at both concentrations hardly decreased the colony number ($P > 0.05$). In short, lycopene had potential chemopreventive effects on carcinogen-induced cutaneous tumor in the promotion phase.

Predicted mechanism for the role of lycopene in the promotion phase of cutaneous tumor

To explore the mechanism for the role of lycopene without blind searching, we utilized a comprehensive method combining bioinformatics, pharmacophore mapping, and network analysis. First, we predicted the putative targets of lycopene by using pharmacophore mapping, a web server for identifying the potential targets of active compounds [26]. According to the fit scores, top 100 putative targets were selected and sorted (Submission ID 160927141728, Supplementary Table 1). In general, compounds for use are determined by the functions of their affected targets that play crucial roles in pathological changes. Therefore, it is equally important to find the key joints of promotion phase of cutaneous tumor. Based on gene expression profiles, we used microarray data available in Array-express (E-MEXP-188) to obtain the preventive signature of promotion phase [27]. In brief, one set of comparison were conducted. DMBA-initiated skin (D) was compared with DMBA-initiated, TPA-promoted skin (DT). This comparison produced a mixed response to the gene expression changes related with the cancer-promoting effects of TPA only. Differentially expressed genes with higher changes ($P< 0.05$, Fold Chang (FC)> 1.5) were considered as significantly altered merely in the promotion phase (Figure 3A). Based on this, networks in which the promotion-related preventive signature interacted with the putative targets of lycopene in a PPI (protein-protein interaction) manner were constructed [28]. Afterwards, the most important targets (candidate targets) were screened by utilizing topological features with a widely used plugin CytoNCA [29] (Supplementary Table 2). The interrelations between functional groups and their significances in biological networks were investigated by enrichment analysis to study the possible roles of these key targets [30]. As displayed in Figure 3B, the targets with topological features are significantly related with intracellular oxidative stress, Nrf2 pathway, and autophagy. This prediction was validated by subsequent experiments.

Lycopene reversed the intracellular redox imbalance induced by carcinogens in vivo and in vitro

As a commonly used tumor promoter, TPA can dramatically accelerate DMBA-induced malignant transformation of preneoplastic cell by inducing redox imbalance [31]. Therefore, we first explored whether this stress was reversed by lycopene pretreatment. As exhibited in Figure 4A–4C, lycopene significantly suppresses all the oxidative damages to lipid (4-HNE) and DNA (8-OHdG) compared to those of the model group in vivo and in vitro, in agreement with the results of ROS accumulation. Lycopene also rebalanced the GSH/GSSG ratio, partly representing the cellular redox condition commendably [32] (Figure 4D). The antioxidant defense enzyme system, including catalase (CAT), glutathione reductase (GR), superoxide dismutase (SOD), and glutathione peroxidase (GPx), essentially maintains cellular redox homeostasis [33]. Accordingly, whether lycopene triggered enzymatic response in the presence of TPA was further studied. As expected, the lower activities of these enzymes were reversed by this compound (Figure 4E). The mRNA levels of GSH and these antioxidant substances were also up-regulated significantly by lycopene pretreatment (Figure 4F). On these basis, the effect of lycopene on

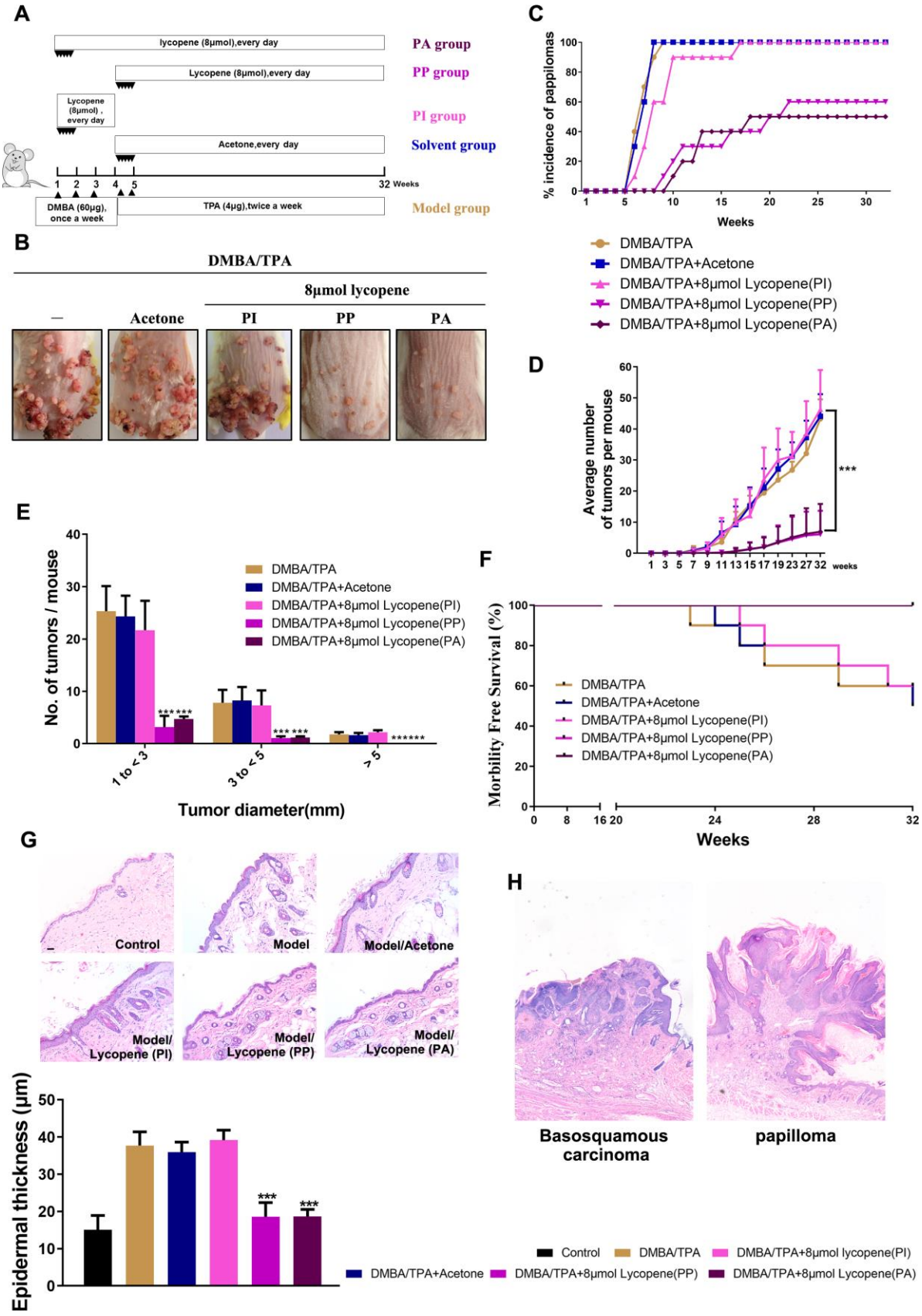

Figure 1. Chemopreventive effect of lycopene on DMBA/TPA-induced cutaneous papilloma in vivo. (**A**) The workflow of animals study as described in results and methods. (**B**) Representative images of papillomas in the indicated groups. (**C**) The incidence of papillomas in

different treatment groups (n=10). (**D**) The average numbers of papillomas per mouse in the indicated groups (n=10). The data are presented as the mean ± SD. ***p < 0.001 (versus DMBA/TPA) (**E**) The average numbers of papillomas per mouse in different tumor diameter groups (n=10). The data are presented as the mean ± SD. ***p < 0.001 (versus DMBA/TPA). (**F**) Survival rates of mice in different treatment groups within 32 weeks. (**G**) Presentative images of epidermal proliferation and hyperplasia in the indicated groups (40×). (Bottom) Quantitative analysis of epidermal thickness based on H&E images (n=6). The data are presented as the mean ± SD. ***p < 0.001 (versus DMBA/TPA). (**H**) (Left panel) Basosquamous carcinoma was observed in mouse in DMBA/TPA model group, and local invasion of basosquamous carcinoma cells can be detected into stroma (40×). (Right panel) Only the benign papillomas can be found in PA and PP mouse with intact basement membranes and hyperplasia of the overlying epidermis (40×).

this antioxidant cell defence system has also been demonstrated in vitro, additionally (Figure 4G–4I), suggesting this compound prevented cutaneous tumor probably by maintaining intracellular redox homeostasis through regulating the antioxidant defense system.

Lycopene activated the Nrf2 pathway in the presence of carcinogens in vivo and in vitro

Considering the vital role of Nrf2 in controlling redox status and in previous enrichment analysis results [34] (Figure 3B), we examined whether the Nrf2 pathway was activated by lycopene. Besides obviously inducing nuclear Nrf2 accumulation in the epidermis (Figure 5A), lycopene also increased nuclear Nrf2 localization in JB6 P+ cells relative to dosage and time (Figure 5B–5E). Subsequently, the transcription and translation of NQO1 and HO-1, two Nrf2 specific target genes, were coordinately up-regulated by lycopene in cutaneous tissue (Figure 5F, 5G). Then JB6 P+ cells were treated by different doses of lycopene without or with TPA, and NQO1 and HO-1 expressions were detected by qPCR. Lycopene pretreatment induced mRNA level of these two genes dose-dependently (Figure 5H) with TPA present. As evidenced by Figures 4 and 5, lycopene indeed enhanced the ability of intracellular

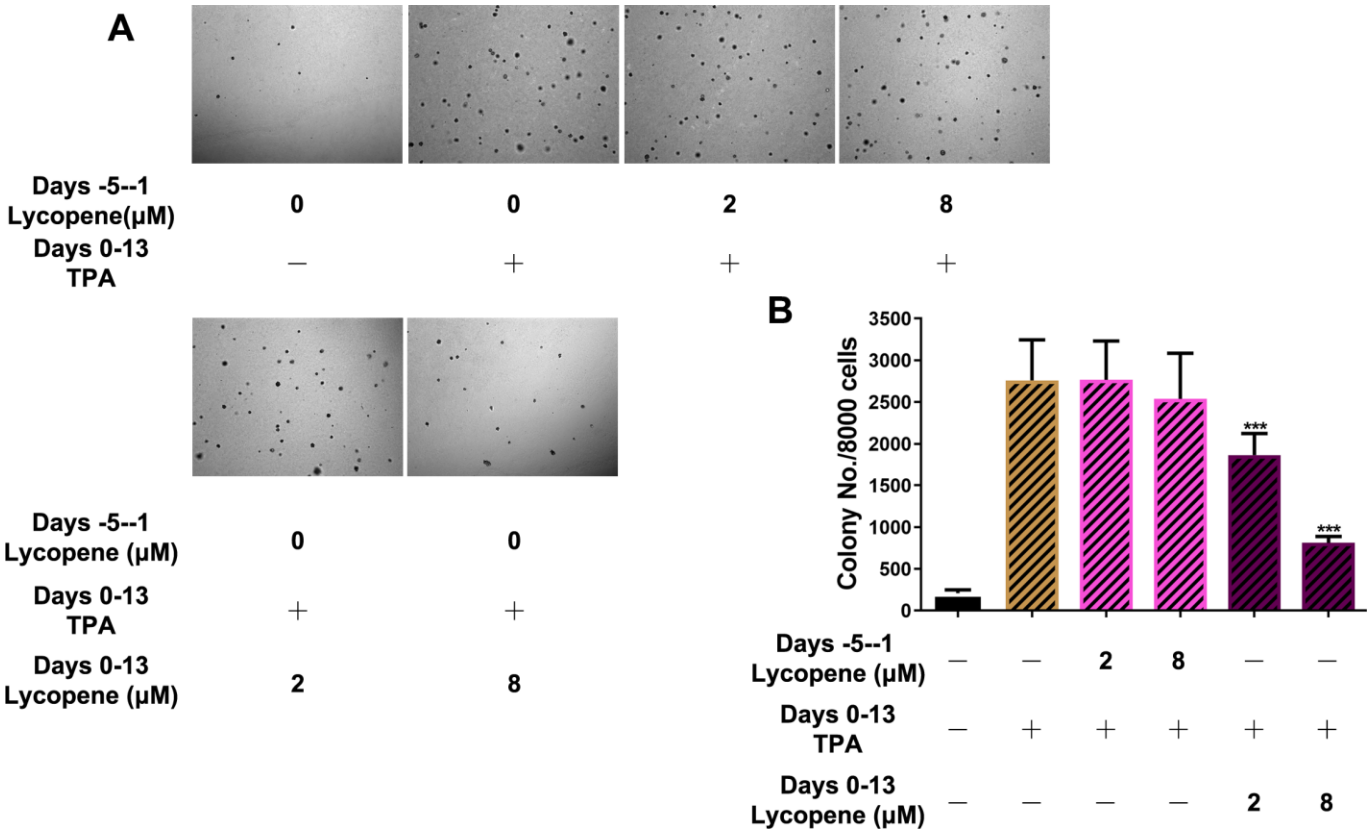

Figure 2. Inhibitory effects of lycopene on TPA-induced transformation of JB6 P+ cells in vitro. (**A**) Soft agar assay of cells with indicated treatment and time. Images were taken and analyzed using the ZEN pro 2012 imaging software on a Zeiss invert microscope under 100-fold magnification. (**B**) Quantitative analysis of the soft agar assay (n=3). The data are presented as the mean ± SD. ***p < 0.001 (versus TPA alone).

defense system to electrophilically and oxidatively, activate the Nrf2 pathway, and effects of which can be dramatically enhanced with TPA present.

Nrf2 was required for lycopene-induced prevention against cutaneous tumor

To study whether Nrf2 was dominantly involved in the influence of lycopene on the promotion phase, cutaneous papilloma was induced in mice by global deletion of Nrf2 using DMBA/TPA. Interestingly, the preventive effects of lycopene on the incidence, multiplicity, and size of cutaneous papilloma induced by DMBA/TPA were reversed considerably (Figure 6A–6D). Moreover, there was no significant change of epidermal thickness in the DMBA/TPA-treated Nrf2-/- group and lycopene-treated group (Figure 6E). The redox imbalance status influenced by the carcinogens in Nrf2 knock-out mice also did not change with lycopene pretreated (Figure 6F–6H). Additionally, we evaluated the influence of lycopene on the malignant transformation of JB6 P+ cells after knock-down by using Nrf2 shRNA. Knock-down of Nrf2 facilitated the growth of JB6-shNrf2 cells in soft agar significantly compared with that of JB6-shMock cells ($P < 0.01$) (Supplementary Figure 1). Moreover, pretreatment with 2-8 μM lycopene significantly suppressed the anchorage-independent growth of JB6-shMock cells induced with TPA. Contrarily, this inhibition was attenuated in JB6-shNrf2 cells. Hence, Nrf2 played a critical role in lycopene-induced prevention against mouse cutaneous tumors due to carcinogen.

Lycopene induced activation of Nrf2 by reducing Keap1 protein at the posttranslational level via the autophagy-lysosomal pathway

As mentioned above, lycopene enhanced the activity of Nrf2 significantly. To unravel the mechanism by which lycopene mediated Nrf2 activation, we firstly studied

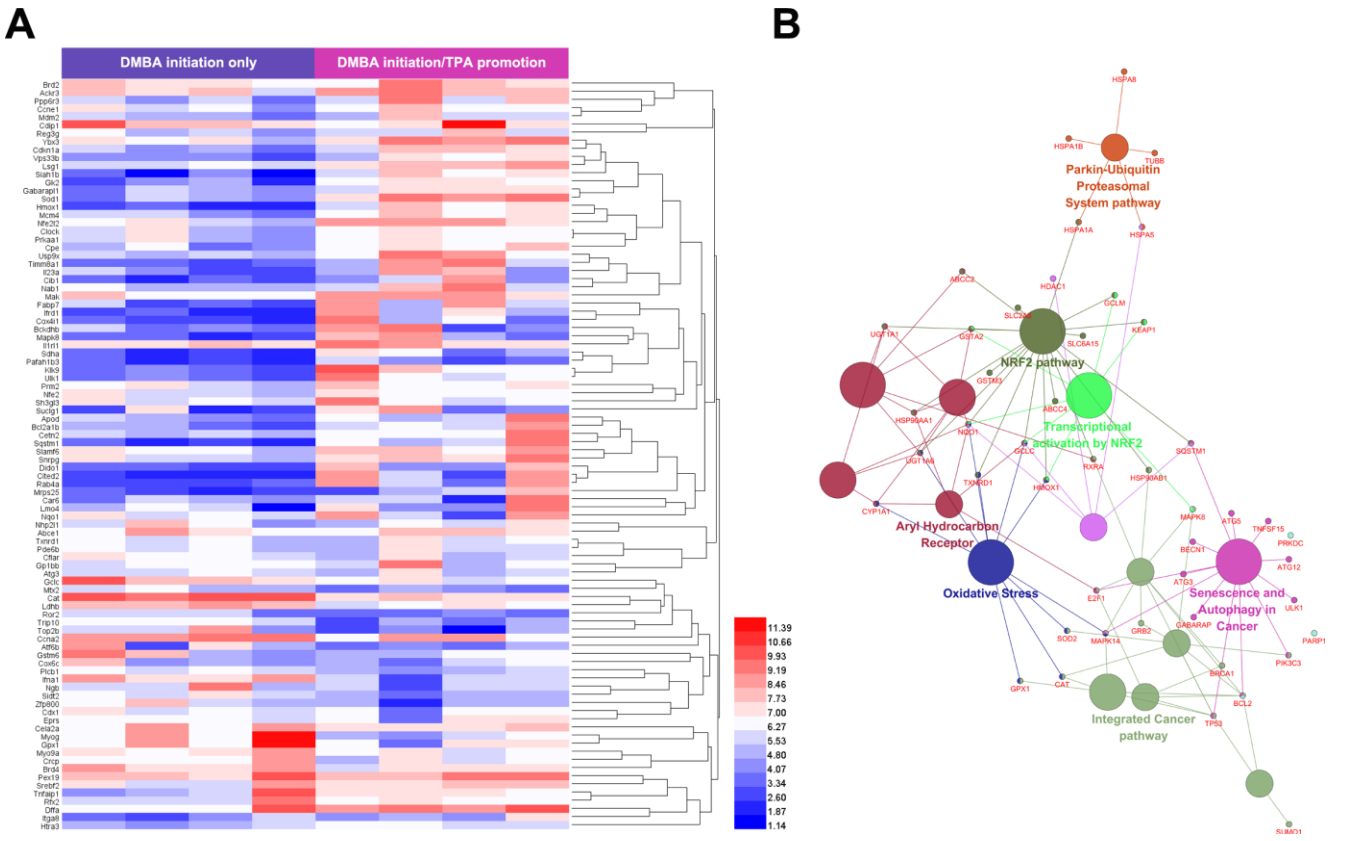

Figure 3. Predicted mechanism for the role of lycopene in the promotion phase of cutaneous tumor. (**A**) Identification of cutaneous tumor related targets by existing microarray data. 92 different expression genes identified were highly related to promotion phase of cutaneous tumor. Upper color bar represents sample classes. P< 0.05, FC>1.5 was considered as the cutoff value. (**B**) ClueGO pathway analysis of the candidate lycopene targets. Functionally grouped network of enriched categories was generated for the target genes. GO terms are represented as nodes, and the node size represents the term enrichment significance. Functionally related groups partially overlap. Only the most significant term in the group was labeled. Representative enriched pathway (P<0.05) interactions among candidate lycopene targets.

whether MAPK and Akt, as kinases that can regulate this pathway and can be phosphorylated by lycopene, participated in this regulatory process [35, 36]. As presented in Figure 7A–7C, lycopene-induced Nrf2 translocation in JB6 P+ cells is not affected by the pharmacological inhibition of either kinase. Dissimilarly, western blot analysis revealed lycopene treatment resulted in a significant increase in the total Nrf2 level (Figure 7D). In addition, we focused on the translational and post-translational regulation of Nrf2 which was evidenced by our observation that lycopene did not alter the mRNA level of Nrf2 (Figure 7E). After cycloheximide (CHX) treatment to block protein synthesis, the Nrf2 levels with or without lycopene were measured over time. As shown in Figure 7F, Nrf2 levels decreased by 100% within 12 h in the presence of CHX alone. Nevertheless, further lycopene treatment reduced the level of Nrf2 protein by less than 75% within 12 h, so lycopene caused Nrf2 enhancement following a posttranslational mechanism.

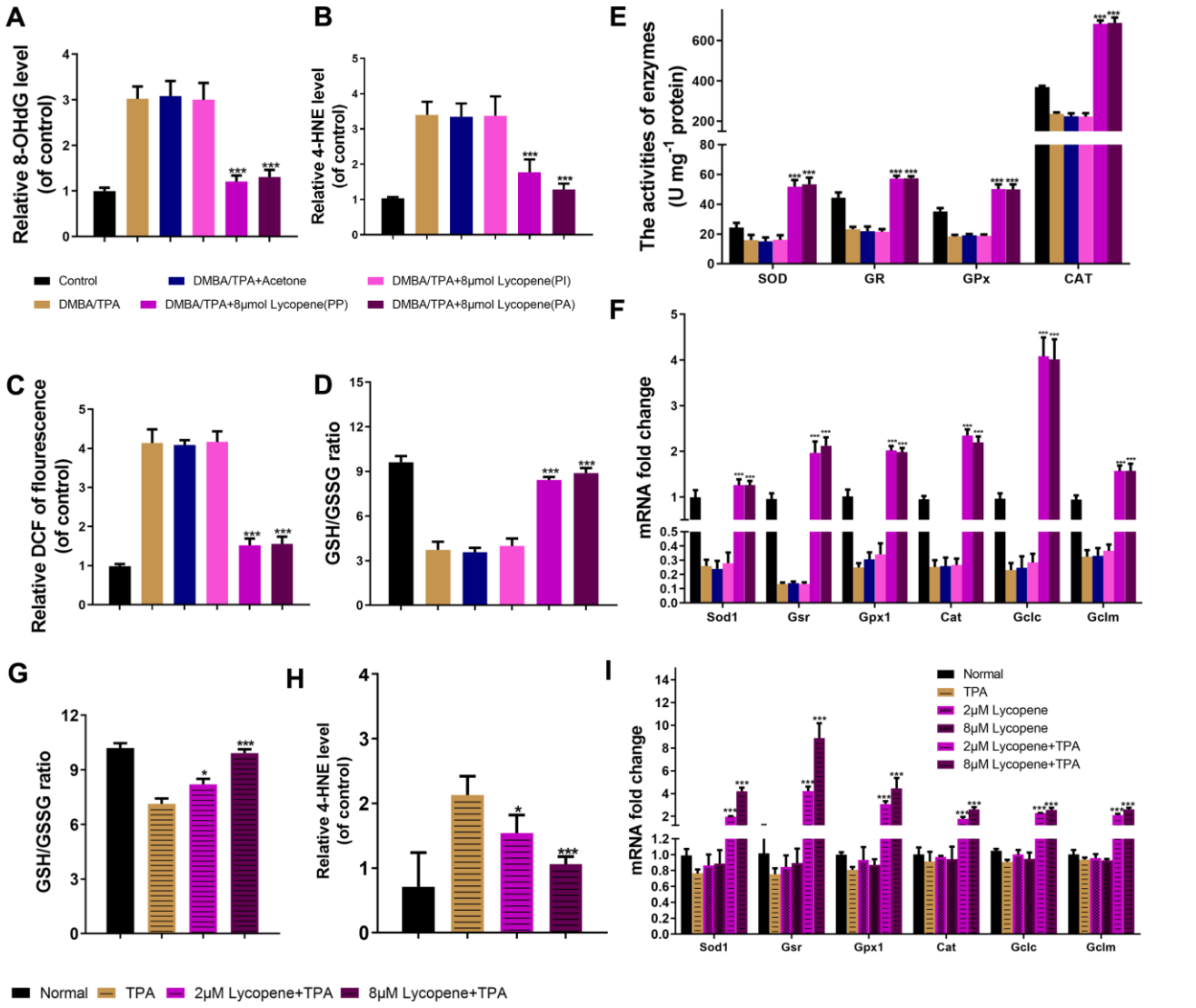

Figure 4. Lycopene reversed the intracellular redox imbalance induced by carcinogens in vivo and in vitro. (**A**, **B**) The level of 8-OhdG, 4-HNE in mouse skin of the indicated groups (n=3). (**C**) The DCFH-DA staining was used to detect ROS production in the indicated groups (n=3). (**D**) The GSH/GSSG ratio in mouse skin of the indicated groups (n=3). (**E**) The activities of SOD, GR, GPx and CAT in mouse skin of the indicated groups (n=3). (**F**) Total mRNA was isolated and analyzed to determine the levels of cat, sod1, gpx1, gsr, gclc and gclm expression using real-time qPCR in mouse skin of the indicated groups (n=3). (**G**) The effect of lycopene on GSH/GSSG ratio in lycopene-pretreated JB6 P+ cells with TPA stimulation (n=3). (**H**) The effect of lycopene on level of 4-HNE in vitro with TPA stimulation (n=3). (**I**) The mRNA levels of cat, sod1, gpx1, gsr, gclc and gclm were detected by real-time qPCR in lycopene-pretreated JB6 P+ cells with TPA stimulation (n=3). House-keeping gene gapdh was used as internal control. The data are presented as the mean ± SD. *p < 0.05, **p < 0.01 and ***p < 0.001 (versus DMBA/TPA or TPA).

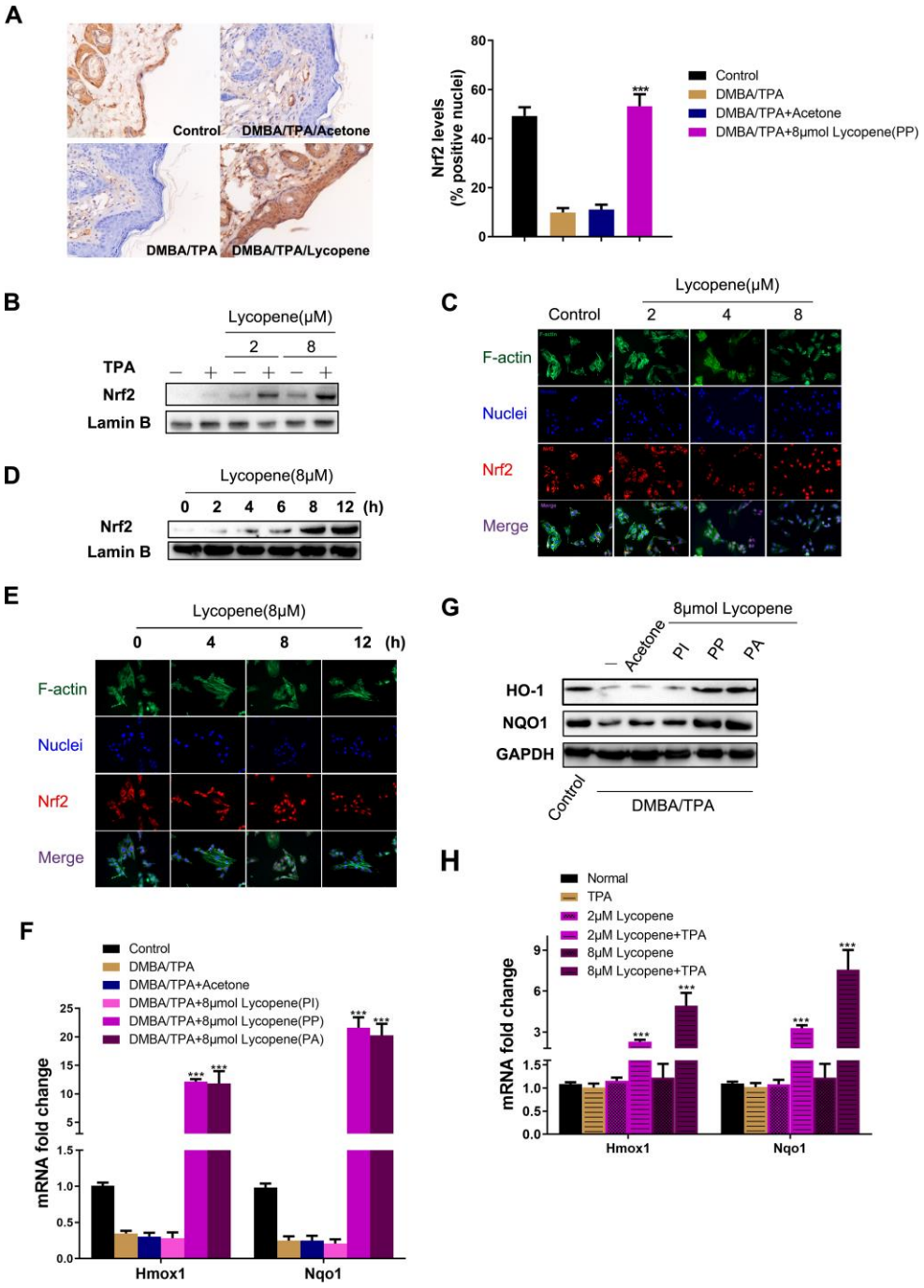

Figure 5. Lycopene activated the Nrf2 pathway in the presence of carcinogens in vivo and in vitro. (**A**) (Left panel) Representative images of Nrf2 immunohistochemistry staining in mouse epidermis in different groups (magnification 100×). (Right panel) Quantitative analysis of Nrf2 IHC results in left panel (n=9 per group). The data are presented as the mean ± SD. ***p < 0.001 (versus DMBA/TPA). (**B**) JB6 P+ cells were pretreated with increasing doses of lycopene for 12 hours and then exposed with or without TPA for additional 2 hours, and the nuclear levels of Nrf2 and LaminB1 were measured by Western blot. LaminB1 was used as the loading control. (**C**) JB6 P+ cells were pretreated with increasing doses of lycopene for 12 hours and then exposed with 20 ng/ml TPA for additional 2 hours. The immunofluorescence staining of Nrf2 was conducted as described in Materials and Methods (blue: nuclei, red: Nrf2, green: F-actin). (**D**) JB6 P+ cells were pretreated with 8 μM lycopene for various times and then exposed with TPA for additional 2 hours, and the nuclear levels of Nrf2 and LaminB1 were measured by Western blot. (**E**) The immunofluorescence staining of Nrf2. Treatment similar to (**D**). (**F**) Quantitative RT-PCR analysis of Nrf2 target genes in the mouse skin of the indicated groups (n=3). The data are presented as the mean ± SD. ***p < 0.001 (versus DMBA/TPA). (**G**) The levels of HO-1 and NQO1 in mouse skin were measured by Western blot. The results were representative of three independent experiments. (**H**) Treatment similar to (**B**), and mRNA levels of Hmox1 and Nqo1 were detected by real-time qPCR. GAPDH was used as the loading control. The data are presented as the mean ± SD. ***p < 0.001 (versus TPA alone).

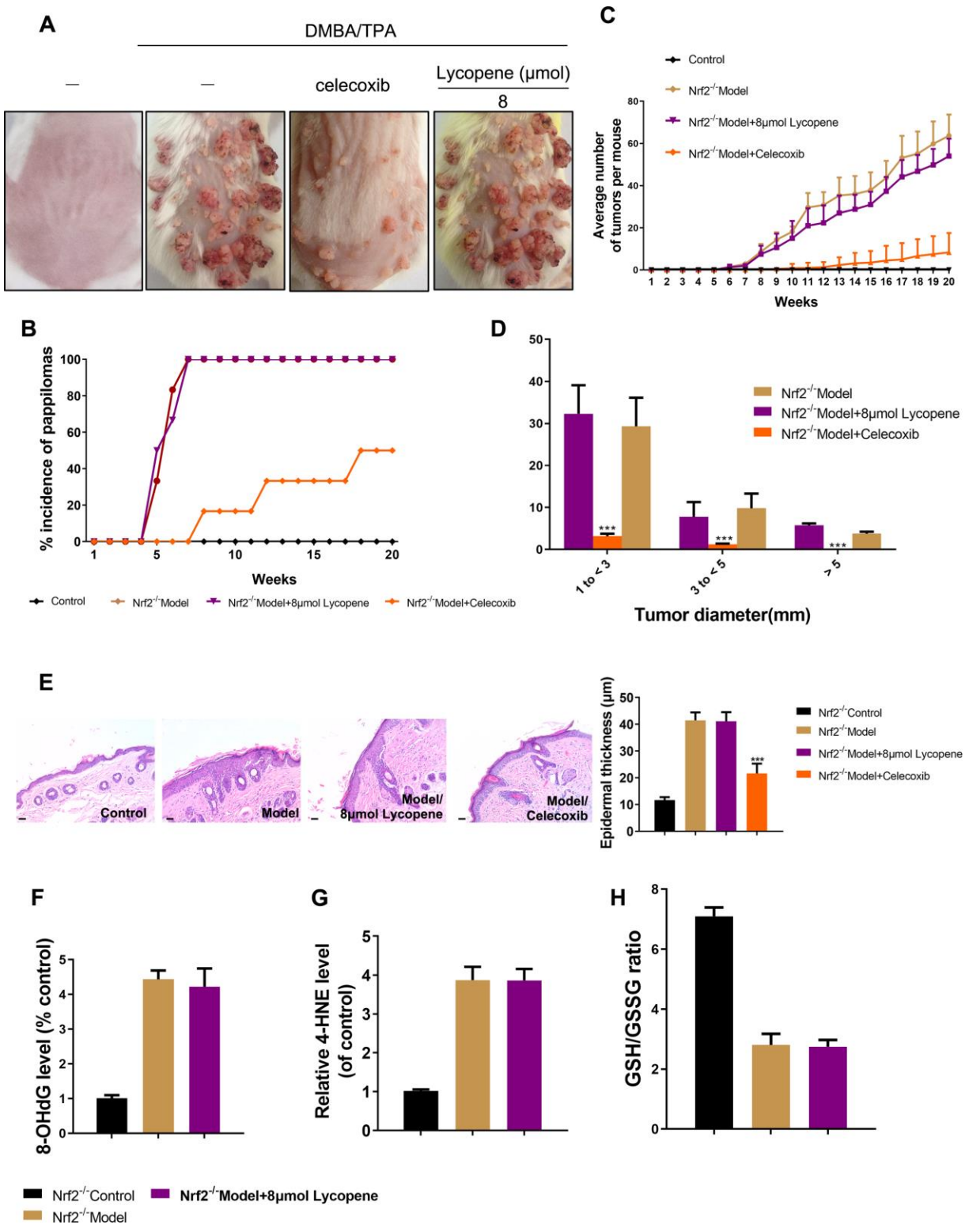

Figure 6. Nrf2 was required for lycopene-induced prevention against cutaneous papilloma. (**A**) Nrf2-/- animals were treated as previous study. Physical appearance of representatives of the indicated groups. (**B**) The incidence of papillomas in different treatment groups (n=6). (**C**) Average numbers of papillomas per mouse from the indicated groups (n=6). (**D**) Average numbers of papillomas per mouse in different tumor diameter groups (n=6). (**E**) Representative H&E staining images of mouse skin in different groups (40×). (Bottom) Quantitative analysis of epidermal thickness in H&E images (n=4). (**F**, **G**) The level of 8-OHdG, 4-HNE in mouse skin tissues of the indicated groups (n=4). (**H**) The GSH/GSSG ratio in mouse skin tissues of the indicated groups (n=4). The data are presented as the mean ± SD. ***p < 0.001 (versus DMBA/TPA).

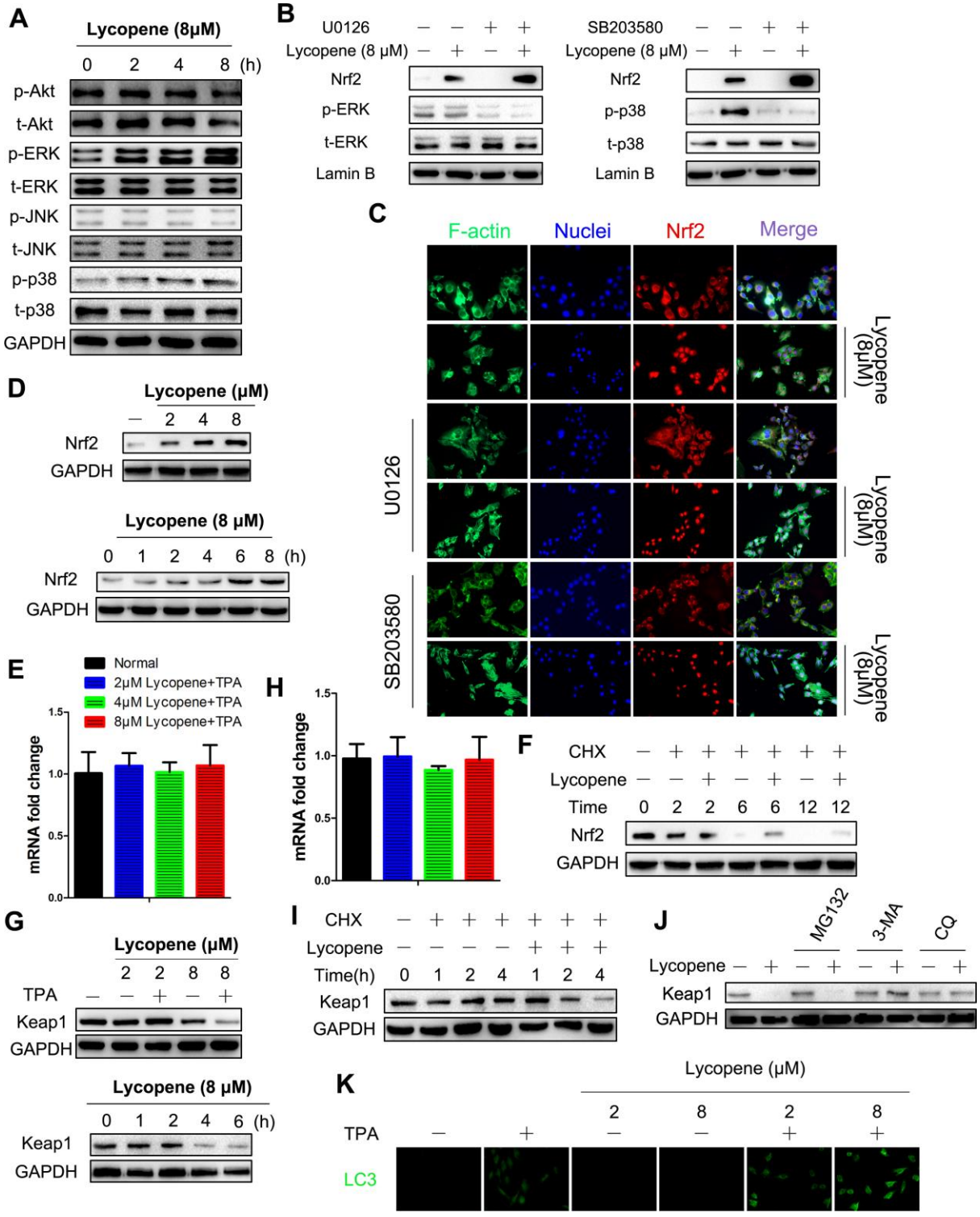

Figure 7. Lycopene induced activation of Nrf2 by reducing Keap1 protein at the posttranslational level via the autophagy-lysosomal pathway. (**A**) Cells were incubated with 8 μM lycopene for the indicated time and then exposed with TPA for additional 2 hours, and the expression of both phosphorylated and total forms of Akt, ERK1/2, p38 and JNK1/2 were measured by western blot analysis. (**B**) Cells were pre-treated with U0126 (left) or SB203580 (right), followed by lycopene treatment for 8 h. The nuclear protein extract was subjected to immunoblot analysis for the detection of Nrf2 expression. (**C**) Immunofluorescence analysis of Nrf2 was carried out as described in Methods. Treatment was similar to (**B**). (**D**) Time-dependent (bottom) and dose-dependent (top) study of lycopene on Nrf2 protein levels. Cells were pretreated with 8 lycopene for different times or with different doses of lycopene for 12 h and then exposed with TPA for additional 2 hours, and the Nrf2 protein level was assayed by Western blot. (**E**) Total RNA was isolated and analyzed to determine the levels of Nfe2l2 mRNA

using real-time qPCR after lycopene treatment for 12 hours. House-keeping gene gaphd was used as the internal control. The data are presented as the mean ± SD. (n=3). (**F**) Cells were pretreated with CHX (0.5 g/ml) alone or in the presence of lycopene (8 μM) and TPA for various times. Nrf2 protein was examined by Western blot. (**G**) Time-dependent (right) and dose-dependent (left) study of lycopene on keap1 protein levels. Cells were pretreated with 8 μM lycopene for different times or with different doses of lycopene for 4 h and then exposed with TPA for additional 2 hours, and the keap1 protein level was assayed by western blot. (**H**) Total RNA was isolated and analyzed to determine the levels of Keap1 expression using real-time qPCR after lycopene treatment for 6 hours. House-keeping gene gapdh was used as the control. The data are presented as the mean ± SD. (n=3). (I) Cells were pretreated with CHX (0.5 g/ml) alone or in the presence of lycopene (8 μM) and TPA for various times. keap1 protein was examined by Western blot. (**J**) Cells were treated with MG132 (1 μM) or 3-MA (1 mM) or CQ (25 μM) for 1 h. Lycopene (8 μM) was added to cells for 6 hours, and then exposed with TPA for additional 2 hours. Expression of keap1 protein was examined by western blot. (**K**) Dose-dependent study of lycopene on LC3 protein levels. Cells were pretreated with different doses of lycopene for 6 h and then exposed with or without TPA for additional 2 hours, and the LC3 was analyzed by immunofluorescent staining. The results are representative blot images of three independent experiments in A, B, D, F, G, I, J, respectively.

As a key inhibitor of Nrf2, Keap1 is the central regulatory protein at the posttranslational level [37]. Lycopene markedly decreased the level of Keap1 protein both time- and dose-dependently (Figure 7G). Keap1 mRNA levels were detected by RT-PCR to elucidate the steps in which lycopene suppressed Keap1 via the Keap1 biosynthesis pathway (Figure 7H). Since this compound did not influence Keap1 mRNA levels, its regulatory role should exist at the transcriptional or posttranscriptional level. By using CHX, we then proved that lycopene induced Keap1 reduction mainly following a posttranslational mechanism (Figure 7I).

Posttranslational protein degradation mainly occurs via the autophagy-lysosomal pathway and the ubiquitin-proteasomal pathway [38]. To determine the pathway with which lycopene induced Keap1 reduction, cells were first treated by lycopene and/or MG132, a ubiquitination-proteasome inhibitor. Keap1 reduction induced by lycopene, which was barely affected by MG132, was blocked by 3-MA, an autophagy inhibitor (Figure 7J). Since 3-MA can affect many cellular processes besides anti-autophagy, we blocked autophagy by using chloroquine (CQ), an autophagosome-lysosome inhibitor. Likewise, cells treated with CQ showed no Keap1 degradation in response to lycopene treatment either (Figure 7J). To further confirm that the autophagy pathway was involved in Keap1 degradation induced by lycopene, we tested the level of LC3-, representing the number of autophagosomes and indicating activation of the autophagy pathway. Lycopene elevated the LC3 level in dose-dependently manner (Figure 7K). Taken together, lycopene mediated the reduction of Keap1 protein via the autophagy degradation pathway.

Lycopene facilitated the interaction between p62 and Keap1 that conferred Keap1 degradation accompanied by Nrf2 stabilization and its preventive effects on cutaneous tumor

To find a direct autophagy-related mediator, we focused on p62 because elevation in its expression can promote p62/Keap1 binding and can compete for Keap1 binding with Nrf2, contributing to activation of the Nrf2 pathway [39]. Figure 8A showed that lycopene raises p62 protein level both dose- and time-dependently, and almost synchronized with Nrf2 increase. As demonstrated by the co-immunoprecipitation assay, lycopene induced p62 binding to Keap1, so Keap1 degradation was mediated by p62 (Figure 8B). To test the role of p62 in Keap1 degradation, p62 was knocked down by using a p62-specific RNA interfering strategy. Knock-down of p62 reversed Keap1 degradation and Nrf2 induction caused by lycopene, supporting that Keap1 degradation was induced by lycopene via the p62-mediated autophagy pathway (Figure 8C). In JB6-shp62 cells, the inhibitory effects of lycopene on the anchorage-independent growth of JB6 P+ cells induced by TPA were weakened (Figure 8D). Collectively, lycopene prevented carcinogen-induced cutaneous tumors mainly by inducing activation of the Nrf2 pathway through p62-triggered autophagic Keap1 degradation.

DISCUSSION

Until now, cutaneous carcinoma remains the most common human malignancy (particularly for the white population) owing to increasing urbanization, rising life expectancy, and lifestyle changes. Millions of new cases are being diagnosed worldwide annually. Even if effective treatment modalities, including chemotherapy, radiotherapy, immunotherapy, photodynamic therapy, and selective inhibitors, have been developed successfully, the burden of cutaneous carcinoma is still chronically high [3]. Alternatively, as one of the most promising approaches that suppress, reverse, or block carcinogenesis in the initiation, promotion, or progression phase, chemoprevention has been widely used to decrease the rates of cutaneous carcinoma incidence and related death [5].

Lycopene, the principle phytochemical found in tomato, also a popular additive in skin-care products, has been found to have multiple associated biological functions for cutaneous tissue, including anti-inflammatory, anti-microbial, and anti-aging effects. For the first time, we

herein found in a DMBA-initiated, TPA-promoted mouse model of cutaneous papilloma that lycopene obviously decreased cancer incidence rate and multiplicity, delayed the latency, and kept the benign nature of tumors only in the promotion phase through a kind of grouping unlike most previous studies. Additionally, most currently available preclinical studies concerning natural compounds were performed by using fully transformed cancer cells in vitro. In this study, we also verified that lycopene prevented the carcinogenesis of pre-malignant JB6 P+ cells in vitro by inhibiting TPA-stimulated malignant transformation. As suggested by the significant reduction of chemically induced tumorigenesis of cutaneous tissues and cells, lycopene may be an eligible cancer chemopreventive agent. Therefore, the mechanisms by which lycopene exerted antitumor effects in vitro and in vivo should be further explored.

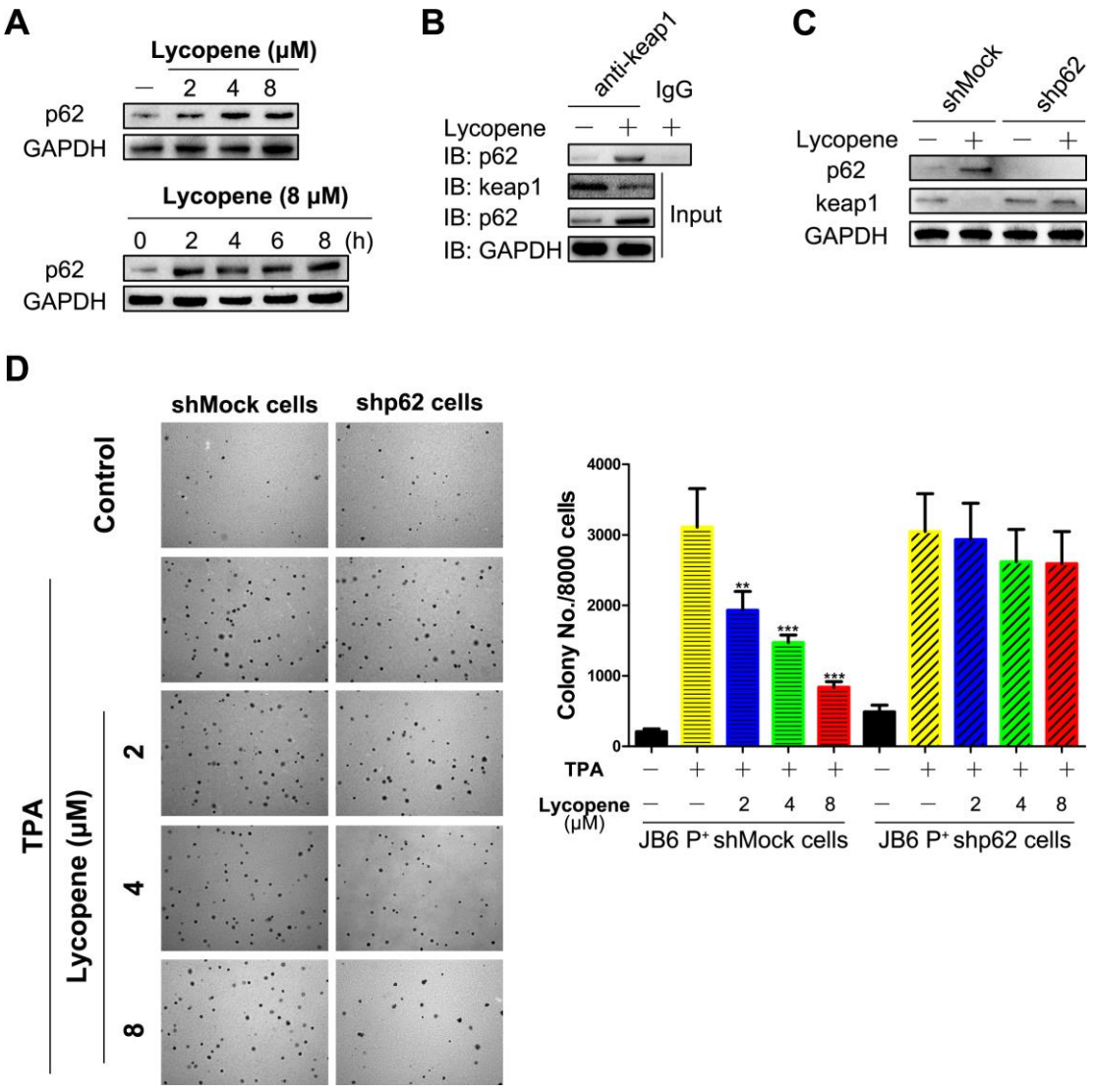

Figure 8. p62 mediates lycopene-induced keap1 degradation and cutaneous tumor prevention. (**A**) Time-dependent (bottom) and dose-dependent (top) study of p62 protein levels. Cells were pretreated with 8 μM lycopene for different times or with different doses of lycopene for 6 hours and then exposed with TPA for additional 2 hours, and the p62 was analyzed by western blot. (**B**) Cells were treated with lycopene for 4 hours and then exposed with TPA for additional 1 hours. Co-IP was done as described in Methods, and the immunoprecipitants were immunoblotted using antibodies for keap1, p62 and GAPDH. (**C**) Cells were transfected with shRNA specific for p62 or a nonspecific control shRNA for hours and then treated with lycopene (8 μM) for 6 hours and then TPA for 2 additional hours. Keap1 and p62 proteins were assayed by Western blot. (**D**) Inhibitory effect of lycopene pretreatment on the TPA-induced transformation of shMock- and shp62-transfected JB6 P+ cells. (right) Quantitative analysis of this soft agar assay (n=3). The data are presented as the mean ± SD. **p < 0.01, ***p < 0.001 (versus TPA alone). The results are representative blot image of three independent experiments shown in **A**, **B**, **C**, respectively.

By using a comprehensive strategy, we predicted that lycopene prevented mouse cutaneous tumors in the promotion phase with association of intracellular autophagy and redox state. As the tumor promoter for the model we used, TPA evidently stimulated the malignant transformation of preneoplastic cells by disruption of redox balance, which was significantly inhibited by lycopene pretreatment both in vitro and in vivo. Furthermore, the antioxidant enzyme defense system was also enhanced by lycopene, suggesting that lycopene exerted preventive effect on cutaneous tumor by keeping intracellular redox homeostasis.

The transcriptional activation of gene-encoding cytoprotective or antioxidant proteins was dominantly regulated by the redox-sensitive transcription factor Nrf2. Lycopene activated the transcription and nuclear translocation of Nrf2, and induced the expression of downstream genes. Interestingly, this effect can be exponentially enhanced with TPA present; suggesting the a primary ability of lycopene to be that of maintaining equilibrium against intracellular stressors caused by carcinogens rather than that of normal cells, and this action model of drugs may lead to a relatively lower adverse reaction. In addition, Nrf2 was crucial for lycopene to maintain cellular redox homeostasis and to relieve tumorigenesis in both gene knock-down cells and transgenic mice.

Lycopene pretreatment induced Nrf2 protein accumulation, but did not change its mRNA level. Nrf2 is a stress-responsive transcription factor that is constantly degraded by the Keap1-Cul3 E3 ubiquitin ligase complex through polyubiquitination [34]. Upon stress challenges, Nrf2 escapes polyubiquitination by this complex and accumulates in the cell nucleus, inducing the transcription of stress-responsive genes. Nrf2 activation by cancer chemopreventive agents has been explained by two plausible mechanisms. One is Keap1 inhibition, and the other is Nrf2 phosphorylation by kinases such as Akt and MAPKs [37]. To clarify the mechanisms underlying lycopene-induced Nrf2 activation, we first focused on the upstream kinases well-documented to participate in the activation of Nrf2 signaling. Lycopene induced the phosphorylation of p38 MAPK and ERK, but blocking these two kinases did not affect nuclear Nrf2 localization, implying that the second mechanism may not be applicable to this study. Based on this, we studied the plausibility of the first mechanism. It is well-established that endogenous

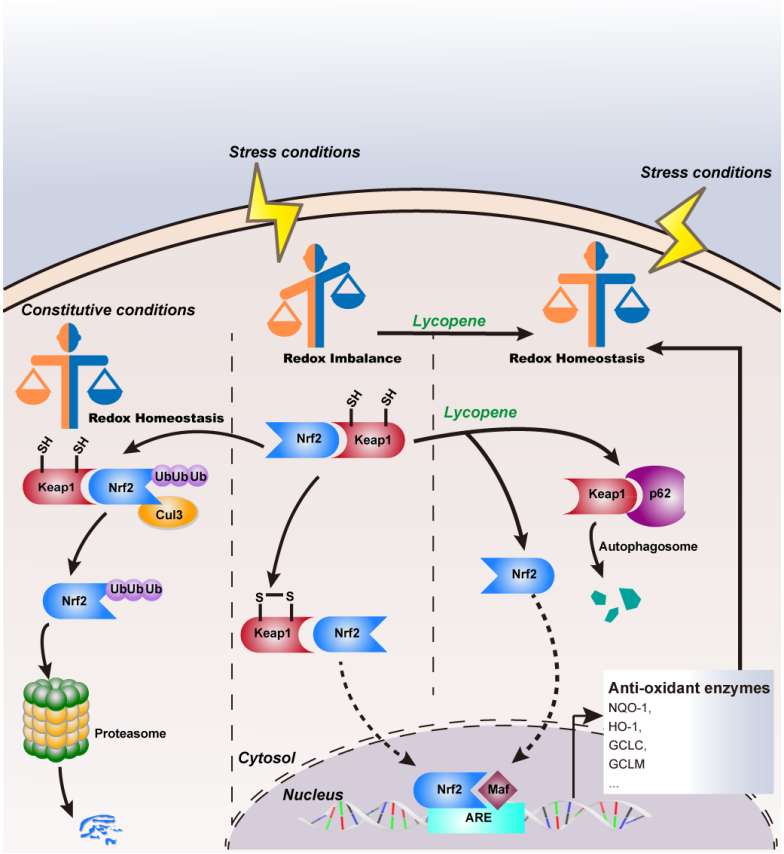

Figure 9. Schematic model of lycopene's inhibitory effects on cutaneous tumor progression.

Keap1 level plays an important role in controlling Nrf2 activity, and that knock-down of Keap1 gene can boost Nrf2 activity and alleviate oxidative stress and steatosis induced by fasting [37]. Lycopene herein induced Keap1 reduction at the protein level, because its mRNA level remained constant. To the best of our knowledge, microbial and cellular components are eliminated mainly by autophagy and ubiquitination to maintain homeostasis. In this study, autophagy mediated the inhibitory effects of lycopene on Keap1 protein. First of all, MG132, a proteasome inhibitor, did not work, but 3-MA and CQ, as specific inhibitors for autophagy, abolished lycopene-induced reduction of Keap1 protein. Secondly, lycopene treatment increased LC3 and LC3-II cleavage and synchronized to the Keap1 degradation.

We herein demonstrated that pretreatment with lycopene induced autophagy by raising p62 protein level and enhancing the binding of p62 to Keap1. In the absence of p62, lycopene did not induce Keap1 degradation. Similarly, knock-down of p62 reversed the inhibitory effects of lycopene on the malignant transformation of JB6 P+ cells induced by TPA, indicating that lycopene prevented cutaneous tumors through inducing the Nrf2 pathway activation by p62-triggered autophagic Keap1 degradation.

In summary (Figure 9), topical lycopene application inhibited TPA-induced intracellular redox imbalance and mouse cutaneous tumors in the promotion phase by accelerating nuclear localization of Nrf2, which may be mediated by up-regulating p62 protein levels, facilitating Keap1 degradation in an autophagy-lysosomal pathway. Based on the results of this study, lycopene or tomato-related skin-care products in combination with protective sun screen may be helpful in reducing skin cancer in humans.

MATERIALS AND METHODS

Chemicals and reagents

Lycopene (Catalog NO. SMB00706-5MG) from sigma for *in vitro* cell model studies. Lycopene (Catalog NO.1370860-500MG) from Sigma for *in vivo* mouse model studies. 7,12-dimethylbenzanthracene (DMBA), cycloheximide (CHX), MG132, chloroquine (CQ), and 3- methyladenine (3-MA) were purchased from Sigma-Aldrich Chemical Co. (St. Louis, USA). 12-O-tetradecanoyl-phorbol 13-acetate (TPA) was obtained from Cayman Chemical Company (Michigan, USA). Fetal bovine serum (FBS), minimum essential medium (MEM), and trypsin-EDTA solution were purchased from Gibco Laboratories. U0126 and SB203580 were bought from Selleck, USA.

Cell line and cell culture

The mouse epidermal cell line, JB6 P+ (JB6 Cl 41-5a), from American Type Culture Collection (ATCC) were maintained in MEM containing 10% FBS in a humidified 5% CO2 atmosphere at 37°C. The JB6 P+ epidermal cells are derived from mouse skin and are regarded as an appropriate cell model for studying the chemopreventive effect and underling mechanisms of lycopene in vitro.

Establishment of carcinogenesis model induced by DMBA/TPA

Female Institute of Cancer Research (ICR) mice aged 6–7 weeks were supplied from Beijing Vital River Laboratory Animal Technology Co., Ltd and housed in climate-controlled quarters with a 12-h light/12-h dark cycle. All experimental procedures were carried out in accordance with the Guide for the Care and Use of Laboratory Animals, and before the animal experiments were carried out, the procedures were approved by the Research Ethical Committee of Nanjing University of Chinese Medicine. ICR mice were randomly divided into five groups, 10 animals per group. The workflow and animal grouping of the in vivo study was depicted in Figure 1A. Specifically, mouse in all the groups were subjected to DMBA (60 μg) dissolved in 0.2 mL topically on the naked backs. The first week after tumor initiation with DMBA, animals were further exposed to TPA (4 μg) twice a week for a total of 32 weeks: Model group (M). Group A (Acetone group) was the vehicle control group. Mice treated with lycopene (8 μmol in 0.2 mL of acetone) were topically applied five times a week with different initiations and durations designed in Figure 1A. Tumors with more than 1 mm diameter were counted every week. Nrf2-/- mice were gifted by Prof. Peng Cao from Jiangsu Province Academy of Chinese Medicine.

Histological assessment

After the animals were sacrificed, the skin tissue was isolated and part of the fresh tissues were fixed in 4% paraformaldehyde and sent for hematoxylin and eosin (H&E) staining. Sections were photographed using the ZEN 2011 imaging software on a Zeiss invert microscope under 40-fold magnification.

Measurement of 8-OhdG, 4-NHE, ROS, GSH/GSSG and antioxidant enzymes activity in tissues

Part of the fresh skin tissues were snap frozen in liquid nitrogen after excision for further process. Measurement was performed using the commercial kits according to manual instructions. The reduced glutathione and oxidized glutathione (GSH/ GSSG) Quantification Kit,

reactive oxygen species (ROS) assay kit, catalase (CAT) activity assay kit, glutathione peroxidase (GPx) assay kit, superoxide dismutase (SOD) assay kit, and glutathione reductase (GR) assay kit were procured from Beyotime, China. The 4-hydroxy-2-nonenal (4-HNE) ELISA kit and 8-hydroxy-2'-deoxyguanosine (8-OhdG) ELISA kit were from Cell Biolabs, USA.

Protein isolation and western blot analysis

Protein lysates of cells or tissue were prepared with RIPA lysis buffer containing protease and phosphatase inhibitors. Nuclear and cytoplasmic cell extracts were prepared using the NE-PER Nuclear and Cytoplasmic Extraction kit (Thermo). Equal amounts of protein lysates (50 μg) were loaded on SDS-PAGE and transferred onto PVDF membranes. After membranes were blocked with 5% skimmed milk at room temperature for 2-3 hours, they were incubated with antibody against Nrf2 (1: 1000, Abcam, Cat.NO. ab137550), p62 (1: 1000, bioworld, Cat.NO. AP6006), Keap1 (1:500, Santa Cruz, Cat.NO. sc-33569), LaminB1 (1: 1000, Abcam, Cat.NO. ab133741), GAPDH (1: 6000, Bioworld Technology, Cat.NO. AP0063), HO-1 (1: 1000, Abclonal, Cat.NO. A1346), and NQO1 (1:1000, Abclonal, Cat.NO. A0047) followed by incubation with goat anti-rabbit IgGs -HRP (1: 10000, Bioworld Biotechnology, Cat.NO. BS 13278). Target proteins were detected by the ECL system (Millipore) and visualized with the ChemiDoc XRS system (Bio-Rad).

Immunohistochemical (IHC) staining

For IHC analysis of Nrf2 protein, mice tissue samples were collected and paraformaldehyde fixed, and paraffin-embedded sections of skin tissues (4 μm thick) were mounted on slides coated with 2-aminopropyltriethoxysilane, baked, deparaffinized, and rinsed with 3% hydrogen peroxide, and then incubated with proteinase K (0.5 mg/mL). After that, these sections were washed and then blocked with StartingBlockTM blocking buffers (Pierce, Rockford, IL, USA) for 5 min and subsequently incubated with an anti-Nrf2 (1: 100, Abcam, Cat.NO. ab137550) polyclonal antibody for 30 min. Finally, the sections were incubated with Streptavidin-Biotin Complex (Solarbio) for 30 min at room temperature, followed by detection with a 3,3-diaminobenzidine tetrahydrochoride solution (chromogen) (ZSGB-BIO) and counterstained with hematoxylin (Solarbio, China). Sections were further mounted with neutral gums. IHC sections were photo-graphed by Mantra 1.01(Perkin Elmer).

Immunofluorescent staining

After JB6 P+ cells seeded and grown on glass cover slips were treated by indicated agents, they were fixed by pre-cold acetone, then rinsed three times with 1× phosphate-buffered saline (PBS). The cells were permeabilized in 0.1% Triton X-100 and incubated with 1% bovine serum albumin (BSA) in 1× PBS to block nonspecific binding. Subsequently, the cells were immunostained by incubating with Nrf2 antibody (1: 100, Abcam, Cat.NO. ab137550) overnight at 4°C. After being washed with PBS, cells were incubated with Rhodamin-conjugated goat anti-rabbit antibody (1: 200, CWBIO, China, Cat.NO. BA1105). Actin filaments were stained using Actin-Tracker Green (Beyotime, China). Nuclei were counterstained with Hoechst 33258 (Beyotime, China). Fluorescent images were taken and analyzed using the ZEN pro 2012 imaging software on a Zeiss invert microscope under 200-fold magnification.

Co-immunoprecipitation assay

For co-immunoprecipitation experiment, cell lysates adjusted to 1 mg/mL protein were precleared by antibody keap1 (1: 20, Santa Cruz, Cat.NO. sc-33569). After gentle rocking at 4°C overnight, Protein A/G PLUS-Agarose (Santa Cruz, Cat.NO. sc-2003) was added to the lysate/antibody mixture, and incubated with gentle agitation at 4°C for 4 h. Then the immunoprecipitates were collected by centrifugation (12000 rpm, 4 min) and washed three times with cell lysis buffer (NP-40, Beyotime), then boiled for 5 min with the same volume of 2× loading buffer (62.5 mM Tris-HCl, pH 6.8, 2% w/v SDS, 10% glycerol, 50 mM DTT, 0.01% w/v bromophenol blue). Protein interactions were analyzed via Immunoblot for p62.

RNA isolation and quantitative real-time PCR

Total RNA was extracted from the tissue samples or cells using the TRIzol reagent (Invitrogen). First-strand cDNA was synthesized with 500 ng total RNA using a Hiscript® II QRTSuperMix (Vazyme, China). Quantitative RT-PCR was performed using the SYBR Green Master kit (Bio-Rad, USA) according to the manufacturer's instructions. The comparative cycle threshold (Ct, 2(-ΔΔCt)) method was applied to quantify the relative gene expression levels. The primers used for qRT-PCR were as follows: gapdh: 5'-GGTTGTCTCC TGCGACTTCA-3' (forward) and 5'-TGGTCCAGGGT TTCTTA CTCC-3' (reverse); cat: 5'-CCCCTATTGCCG TTCGATTCT-3' (forward) and 5'-TTCAGGTGAGTC TGTGGGTTT-3' (reverse); sod1: 5'-AACCAGTTGTG TTG TCAGGAC-3' (forward) and 5'-CCACCATGTTT CTTAGAGTGAGG-3' (reverse); gsr: 5'-GCGTGAAT GTTGGATGTGTACC-3' (forward) and 5'-GTTGC AT AGCCGTGGATAATTTC-3' (reverse); gpx1: 5'-AGTC CACCGTGTATGCCTTCT-3' (forward) and 5'-GAGA CGCGACATTCTCAATGA-3' (reverse); gclc: 5'-GGG GTGACGAGGTGGAGTA-3' (forward) and 5'-GTTG

GGGTTTGTCCTCTC CC-3' (reverse); gclm: 5'-AGG AGCTTCGGGACTGTATCC-3' (forward) and 5'-GG GACATGGTGCATTCCAAAA-3' (reverse); hmox1: 5'-CACGCATA TACCCGCTACCT-3' (forward) and 5'-CCAGAGTGTTCATTCGAGCA-3' (reverse); nqo1: 5'-TTCTCTGGCCGATTCAGAGT-3' (forward) and 5'-GGCTGCT TGGAGCAAAATAG-3' (reverse); nfe2l2: 5'-CTCGCTGGAAAAAGAAGTGG-3' (forward) and 5'-CCGTCCAGGAGTTCAGAGAG-3' (reverse); keap1: 5'-TGCCCCTGTGGTCAAAGTG-3' (forward) and 5'G GTTCGGTTACC GTCCTGC-3' (reverse).

shRNA knockdown

Predesigned Nrf2-knockdown shRNA construct and p62-knockdown shRNA construct were purchased from Sigma-Aldrich with Catalog NO. SHCLNG-NM_ 010902_TRCN0000054658 and SHCLNG-NM_011018 _TRCN0000098619, respectively. Vehicle control construct was also provided from Sigma-Aldrich. The sequences for the mouse NRF2-shRNA are CC GGCCAAAGCTAGTATAGCAATAACTCGAGTTA TTGCTATACTAGCTTTGGTTTTTG. The sequences for the mouse p62-shRNA are CCGGGAGGTTG ACATTGATGTGGAACTCGAGTTCCACATCAATG TCAACCTCTTTTTG. The plasmid was transfected using lipofectamine 2000 according to manual's instructions.

Data collection and analysis of target genes related to the promotion phase of cutaneous carcinoma

Microarray data with accession number E-MEXP-188 was downloaded from the Arrayexpress database (http://www.ebi.ac.uk/arrayexpress/) [27]. In brief, one set of comparison were conducted. DMBA-initiated skin (D) was compared with DMBA-initiated, TPA-promoted skin (DT). Different expression genes (DEGs) were defined, and $P< 0.05$, Fold Chang (FC) > 1.5 was considered as the cutoff value.

Protein-protein interaction (PPI) network construction

PPI data was imported from six currently available PPI databases including the Biological General Repository for Interaction Datasets (BioGRID: https://thebiogrid.org), the Biomolecular Interaction Network Database (BIND: http://binddb.org), the Molecular Interaction Database (MINT: http://mint.bio.uniroma2.it/mint/), the Human Protein Reference Database (HPRD: http://www.hprd.org), the Database of Interacting Proteins (DIP: http://dip.doe-mbi.ucla.edu/dip/Main.cgi), and the Biological General Repository for Interaction Datasets by BisoGenet, a Cytoscape plugin [40].

Definition of topological feature set for the network

By calculating six measures (i.e. degree centrality (DC), betweenness centrality (BC), closeness centrality (CC), eigenvector centrality (EC), network centrality (NC), and local average connectivity(LAC)) with CytoNCA, a Cytoscape plugin, the topological property of every node in the interaction network was analyzed [29]. The definitions and computation equations of these six parameters represent the topological importance of a node in the network. The higher the quantitative values of these parameters, the more important the node in this network.

Prediction of drug targets for lycopene

The potential targets of lycopene were predicted using PharmMapper server (provided by the Shanghai Institute of Materia Medica, Chinese Academy of Sciences) [26], a web server for potential drug targets identification using pharmacophore mapping approach at http://59.78.96.61/pharmmapper. Briefly, 3D Mol2 file of lycopene (PubChem CID: 12305761) was submitted to PharmMapper server. During the procedure, the maximum conformations were set up to 300, and the number of reserved matched targets was 1000. Other parameters were kept as default. The submission ID can be stored and used to check the prediction results.

Enrichment analysis

As a Cytoscape plugin visualizing the non-redundant biological terms for large gene clusters in a functionally grouped network, ClueGO was utilized to visualize the enrichment of lycopene candidate targets [30]. The ClueGO network was created by using kappa statistics, reflecting the relationships between the terms on the basis of the similarity between their associated genes. The significances of the terms and groups were calculated automatically.

Statistical analysis

Values were expressed as the mean ± SD of at least three independent experiments. One way analysis of variance (ANOVA) was used to compare in groups and $p < 0.05$ was considered as statistically significant.

Abbreviations

3-MA: 3-Methyladenine; 4-HNE: 4-Hydroxynonenal; 8-OHdG: 8-hydroxy-2'-deoxyguanosine; ANOVA: one way analysis of variance; BC: betweenness centrality; BSA: bovine serum albumin; CAT: catalase; CC: closeness centrality; CHX: cycloheximide; CQ: chloroquine; DC:

degree centrality; DMBA: 7, 12-dimethylbenzanthracene; EC: eigenvector centrality; ELISA: enzyme linked immunosorbent assay; FBS: fetal bovine serum; GPx: glutathione peroxidase; GR: glutathione reductase; GSH: glutathione; GSSG: Glutathione disulfide; Keap1: Kelch ECH associating protein 1; LAC: local average connectivity; MAPK: mitogen-activated protein kinase; MEM: minimum essential medium; NC: network centrality; Nrf2: nuclear factor erythroid 2-related factor 2; PA: pretreatment in all phases; PBS: phosphate-buffered saline; PCR: polymerase chain reaction; PI: pretreatment only before initiation; PP: pretreatment only before promotion; PPI: protein-protein interaction; PVDF: polyvinylidene difluoride; ROS: reactive oxygen species; SCC: squamous cell carcinoma; SDS-PAGE: sodium dodecyl sulfate-polyacrylamide gel electrophoresis; SOD: superoxide dismutase; TPA: 12-O-tetradecanoylphorbol-13-acetate; UV: ultraviolet.

AUTHOR CONTRIBUTIONS

conceptualization, S.W., Y.Y.W, and Y.L.; methodology, S.W. and X.W.; experiment performance and validation, S.W., P.S., Q.J., and S.Y.; formal analysis, S.W., and X.W.; data curation, S.W.; writing, original draft preparation, S.W.; writing review and editing, Y.Y.W., and Y. W.; supervision, W.C., A.W., and Y.L.; project administration, A.W.; funding acquisition, Y.L., A.W, W. C., X. L., and Y.Y.W.

ACKNOWLEDGMENTS

We thank Prof. Peng Cao (Jiangsu Province Academy of Chinese Medicine) for providing Nrf2-/- mice.

CONFLICTS OF INTEREST

The authors declare no conflicts of interest.

FUNDING

This research was funded by National Natural Science Foundation of China (grant number 81703765, 81973734, 81973587, 81673648, 81903857, 81803916), Natural Science Foundation of Jiangsu Province (grant No. BK20180128), Jiangsu College Graduate Research and Innovation Projects (grant number KYZZ15_0271) and Fundamental Research Funds for the Central Universities.

REFERENCES

1. Deady S, Sharp L, Comber H. Increasing skin cancer incidence in young, affluent, urban populations: a challenge for prevention. Br J Dermatol. 2014; 171:324–31. https://doi.org/10.1111/bjd.12988 PMID:24666396

2. Whiteman DC, Green AC, Olsen CM. The Growing Burden of Invasive Melanoma: Projections of Incidence Rates and Numbers of New Cases in Six Susceptible Populations through 2031. J Invest Dermatol. 2016; 136:1161–71. https://doi.org/10.1016/j.jid.2016.01.035 PMID:26902923

3. Simões MC, Sousa JJ, Pais AA. Skin cancer and new treatment perspectives: a review. Cancer Lett. 2015; 357:8–42. https://doi.org/10.1016/j.canlet.2014.11.001 PMID:25444899

4. Savoia P, Cremona O, Fava P. New Perspectives in the Pharmacological Treatment of Non-Melanoma Skin Cancer. Curr Drug Targets. 2016; 17:353–74. https://doi.org/10.2174/1389450116666150806123717 PMID:26245477

5. The Lancet. Skin cancer: prevention is better than cure. Lancet. 2014; 384:470. https://doi.org/10.1016/S0140-6736(14)61320-9 PMID:25110266

6. Uzarska M, Czajkowski R, Schwartz RA, Bajek A, Zegarska B, Drewa T. Chemoprevention of skin melanoma: facts and myths. Melanoma Res. 2013; 23:426–33. https://doi.org/10.1097/CMR.0000000000000016 PMID:24077511

7. Stice CP, Xia H, Wang XD. Tomato lycopene prevention of alcoholic fatty liver disease and hepatocellular carcinoma development. Chronic Dis Transl Med. 2018; 4:211–24. https://doi.org/10.1016/j.cdtm.2018.11.001 PMID:30603740

8. Ilic D. Lycopene for the prevention and treatment of prostate disease. Recent Results Cancer Res. 2014; 202:109–14. https://doi.org/10.1007/978-3-642-45195-9_13 PMID:24531784

9. Wang J, Zou Q, Suo Y, Tan X, Yuan T, Liu Z, Liu X. Lycopene ameliorates systemic inflammation-induced synaptic dysfunction via improving insulin resistance and mitochondrial dysfunction in the liver-brain axis. Food Funct. 2019; 10:2125–37. https://doi.org/10.1039/C8FO02460J PMID:30924473

10. Chen D, Huang C, Chen Z. A review for the pharmacological effect of lycopene in central nervous system disorders. Biomed Pharmacother. 2019; 111:791–801. https://doi.org/10.1016/j.biopha.2018.12.151 PMID:30616078

11. Jorgenson TC, Zhong W, Oberley TD. Redox imbalance and biochemical changes in cancer. Cancer Res. 2013; 73:6118–23. https://doi.org/10.1158/0008-5472.CAN-13-1117 PMID:23878188

12. Mateu-Jiménez M, Sánchez-Font A, Rodríguez-Fuster A, Aguiló R, Pijuan L, Fermoselle C, Gea J, Curull V, Barreiro E. Redox Imbalance in Lung Cancer of Patients with Underlying Chronic Respiratory Conditions. Mol Med. 2016; 22:85–98. https://doi.org/10.2119/molmed.2015.00199 PMID:26772773

13. Kroemer G, Mariño G, Levine B. Autophagy and the integrated stress response. Mol Cell. 2010; 40:280–93. https://doi.org/10.1016/j.molcel.2010.09.023 PMID:20965422

14. Hayes JD, McMahon M. Molecular basis for the contribution of the antioxidant responsive element to cancer chemoprevention. Cancer Lett. 2001; 174:103–13. https://doi.org/10.1016/S0304-3835(01)00695-4 PMID:11689285

15. Dhar SK, Xu Y, Noel T, St Clair DK. Chronic exposure to 12-O-tetradecanoylphorbol-13-acetate represses sod2 induction in vivo: the negative role of p50. Carcinogenesis. 2007; 28:2605–13. https://doi.org/10.1093/carcin/bgm163 PMID:17652337

16. Xu C, Huang MT, Shen G, Yuan X, Lin W, Khor TO, Conney AH, Kong AN. Inhibition of 7,12-dimethylbenz(a)anthracene-induced skin tumorigenesis in C57BL/6 mice by sulforaphane is mediated by nuclear factor E2-related factor 2. Cancer Res. 2006; 66:8293–96. https://doi.org/10.1158/0008-5472.CAN-06-0300 PMID:16912211

17. Shen C, Wang S, Shan Y, Liu Z, Fan F, Tao L, Liu Y, Zhou L, Pei C, Wu H, Tian C, Ruan J, Chen W, et al. Chemomodulatory efficacy of lycopene on antioxidant enzymes and carcinogen-induced cutaneum carcinoma in mice. Food Funct. 2014; 5:1422–31. https://doi.org/10.1039/C4FO00035H PMID:24781038

18. Beyer TA, Auf dem Keller U, Braun S, Schäfer M, Werner S. Roles and mechanisms of action of the Nrf2 transcription factor in skin morphogenesis, wound repair and skin cancer. Cell Death Differ. 2007; 14:1250–54. https://doi.org/10.1038/sj.cdd.4402133 PMID:17380153

19. Moon EJ, Giaccia A. Dual roles of NRF2 in tumor prevention and progression: possible implications in cancer treatment. Free Radic Biol Med. 2015; 79:292–99. https://doi.org/10.1016/j.freeradbiomed.2014.11.009 PMID:25458917

20. Deretic V, Levine B. Autophagy, immunity, and microbial adaptations. Cell Host Microbe. 2009; 5:527–49. https://doi.org/10.1016/j.chom.2009.05.016 PMID:19527881

21. White E. Deconvoluting the context-dependent role for autophagy in cancer. Nat Rev Cancer. 2012; 12:401–10. https://doi.org/10.1038/nrc3262 PMID:22534666

22. Sumpter R Jr, Levine B. Selective autophagy and viruses. Autophagy. 2011; 7:260–65. https://doi.org/10.4161/auto.7.3.14281 PMID:21150267

23. Ichimura Y, Waguri S, Sou YS, Kageyama S, Hasegawa J, Ishimura R, Saito T, Yang Y, Kouno T, Fukutomi T, Hoshii T, Hirao A, Takagi K, et al. Phosphorylation of p62 activates the Keap1-Nrf2 pathway during selective autophagy. Mol Cell. 2013; 51:618–31. https://doi.org/10.1016/j.molcel.2013.08.003 PMID:24011591

24. Fan W, Tang Z, Chen D, Moughon D, Ding X, Chen S, Zhu M, Zhong Q. Keap1 facilitates p62-mediated ubiquitin aggregate clearance via autophagy. Autophagy. 2010; 6:614–21. https://doi.org/10.4161/auto.6.5.12189 PMID:20495340

25. Ishikawa TO, Kumar IP, Machado HB, Wong KP, Kusewitt D, Huang SC, Fischer SM, Herschman HR. Positron emission tomography imaging of DMBA/TPA mouse skin multi-step tumorigenesis. Mol Oncol. 2010; 4:119–25. https://doi.org/10.1016/j.molonc.2010.01.005 PMID:20171942

26. Liu X, Ouyang S, Yu B, Liu Y, Huang K, Gong J, Zheng S, Li Z, Li H, Jiang H. PharmMapper server: a web server for potential drug target identification using pharmacophore mapping approach. Nucleic Acids Res. 2010 (Web Server Issue); 38:W609–14. https://doi.org/10.1093/nar/gkq300 PMID:20430828

27. Ridd K, Zhang SD, Edwards RE, Davies R, Greaves P, Wolfreys A, Smith AG, Gant TW. Association of gene expression with sequential proliferation, differentiation and tumor formation in murine skin. Carcinogenesis. 2006; 27:1556–66. https://doi.org/10.1093/carcin/bgl007 PMID:16537558

28. Chuang HY, Lee E, Liu YT, Lee D, Ideker T. Network-based classification of breast cancer metastasis. Mol Syst Biol. 2007; 3:140.

https://doi.org/10.1038/msb4100180
PMID:17940530

29. Tang Y, Li M, Wang J, Pan Y, Wu FX. CytoNCA: a cytoscape plugin for centrality analysis and evaluation of protein interaction networks. Biosystems. 2015; 127:67–72. https://doi.org/10.1016/j.biosystems.2014.11.005 PMID:25451770

30. Bindea G, Mlecnik B, Hackl H, Charoentong P, Tosolini M, Kirilovsky A, Fridman WH, Pagès F, Trajanoski Z, Galon J. ClueGO: a Cytoscape plug-in to decipher functionally grouped gene ontology and pathway annotation networks. Bioinformatics. 2009; 25:1091–93. https://doi.org/10.1093/bioinformatics/btp101 PMID:19237447

31. Liu Z, Shen C, Tao Y, Wang S, Wei Z, Cao Y, Wu H, Fan F, Lin C, Shan Y, Zhu P, Sun L, Chen C, et al. Chemopreventive efficacy of menthol on carcinogen-induced cutaneous carcinoma through inhibition of inflammation and oxidative stress in mice. Food Chem Toxicol. 2015; 82:12–18. https://doi.org/10.1016/j.fct.2015.04.025 PMID:25956868

32. Jones DP. Redox potential of GSH/GSSG couple: assay and biological significance. Methods Enzymol. 2002; 348:93–112. https://doi.org/10.1016/S0076-6879(02)48630-2 PMID:11885298

33. Zhang HJ, Doctrow SR, Xu L, Oberley LW, Beecher B, Morrison J, Oberley TD, Kregel KC. Redox modulation of the liver with chronic antioxidant enzyme mimetic treatment prevents age-related oxidative damage associated with environmental stress. FASEB J. 2004; 18:1547–49. https://doi.org/10.1096/fj.04-1629fje PMID:15319374

34. Tummala KS, Kottakis F, Bardeesy N. NRF2: Translating the Redox Code. Trends Mol Med. 2016; 22:829–31. https://doi.org/10.1016/j.molmed.2016.08.002 PMID:27555347

35. Shi X, Zhou B. The role of Nrf2 and MAPK pathways in PFOS-induced oxidative stress in zebrafish embryos. Toxicol Sci. 2010; 115:391–400. https://doi.org/10.1093/toxsci/kfq066 PMID:20200220

36. Koyani CN, Kitz K, Rossmann C, Bernhart E, Huber E, Trummer C, Windischhofer W, Sattler W, Malle E. Activation of the MAPK/Akt/Nrf2-Egr1/HO-1-GCLc axis protects MG-63 osteosarcoma cells against 15d-PGJ2-mediated cell death. Biochem Pharmacol. 2016; 104:29–41. https://doi.org/10.1016/j.bcp.2016.01.011 PMID:26801686

37. Niture SK, Khatri R, Jaiswal AK. Regulation of Nrf2-an update. Free Radic Biol Med. 2014; 66:36–44. https://doi.org/10.1016/j.freeradbiomed.2013.02.008 PMID:23434765

38. Wang H, Khor TO, Saw CL, Lin W, Wu T, Huang Y, Kong AN. Role of Nrf2 in suppressing LPS-induced inflammation in mouse peritoneal macrophages by polyunsaturated fatty acids docosahexaenoic acid and eicosapentaenoic acid. Mol Pharm. 2010; 7:2185–93. https://doi.org/10.1021/mp100199m PMID:20831192

39. Komatsu M, Kurokawa H, Waguri S, Taguchi K, Kobayashi A, Ichimura Y, Sou YS, Ueno I, Sakamoto A, Tong KI, Kim M, Nishito Y, Iemura S, et al. The selective autophagy substrate p62 activates the stress responsive transcription factor Nrf2 through inactivation of Keap1. Nat Cell Biol. 2010; 12:213–23. https://doi.org/10.1038/ncb2021 PMID:20173742

40. Martin A, Ochagavia ME, Rabasa LC, Miranda J, Fernandez-de-Cossio J, Bringas R. BisoGenet: a new tool for gene network building, visualization and analysis. BMC Bioinformatics. 2010; 11:91. https://doi.org/10.1186/1471-2105-11-91 PMID:20163717

SUPPLEMENTARY MATERIALS

Supplementary Figure

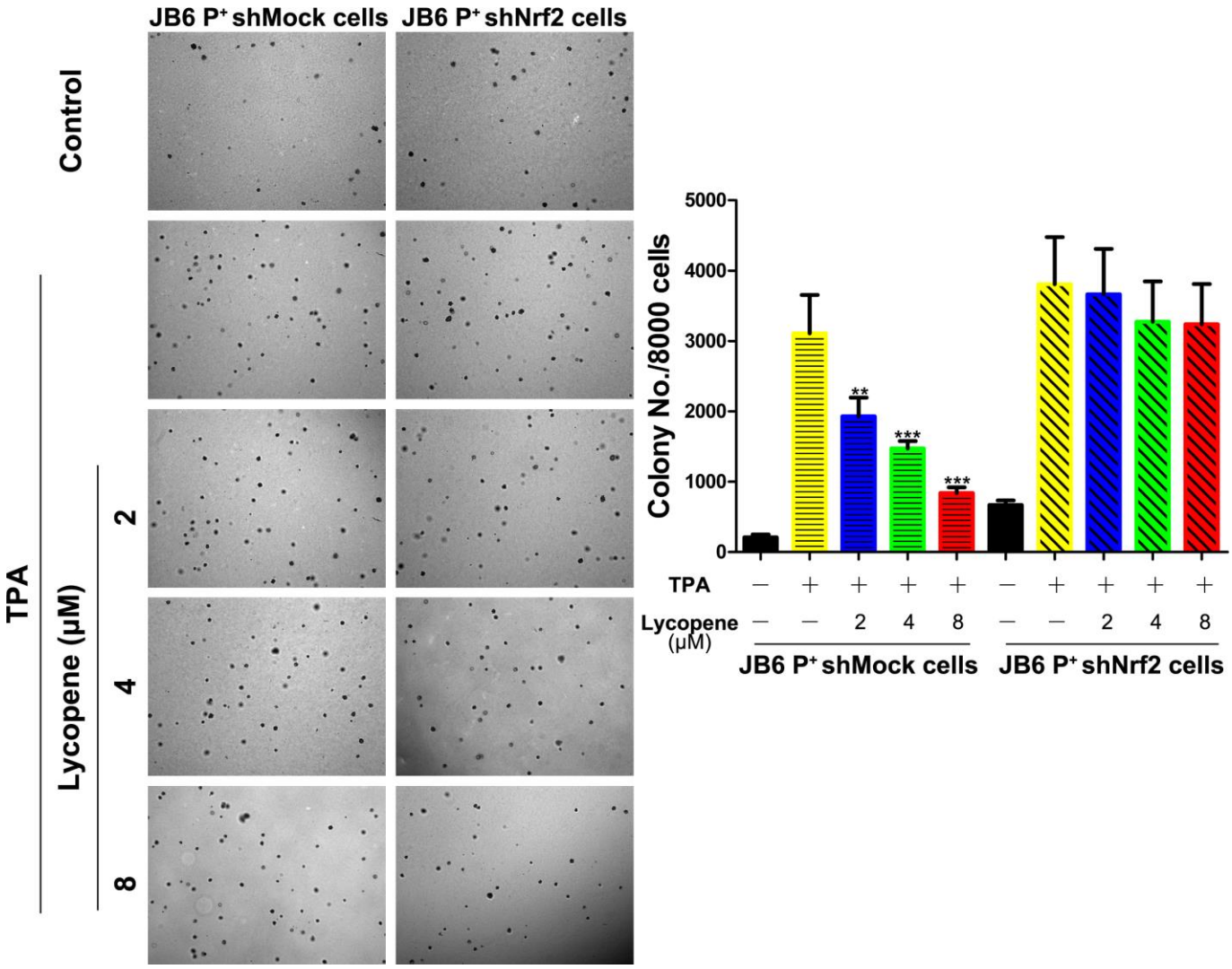

Supplementary Figure 1. Inhibitory effect of lycopene pretreatment on the TPA-induced transformation of shMock- and shNrf2-transfected JB6 P+ cells. Cells (1×10^5/10-cm dish) were treated with lycopene (0–8μM) for 5 days. The pretreated cells (at a density of 8,000 cells/well) were then transferred to soft agar containing TPA in 6-well plates for an additional 2 weeks. The colonies exhibiting anchorage-independent growth were taken and analyzed using the ZEN pro 2012 imaging software on a Zeiss invert microscope under 100-fold magnification. (right) Quantitative analysis of this soft agar assay (n=3). The data are presented as the mean ± SD. $^{**}p < 0.01$, $^{***}p < 0.001$ (versus TPA alone).

Supplementary Tables

Supplementary Table 1. Putative targets of lycopene.

Target name	Targets Gene name	Uniprot ID
GTPase Hras	HRAS	P01112
Inositol monophosphatase1	IMPA1	P29218
Adenosine kinase	ADK	P55263
Beta-hexosaminidase beta chain	HEXB	P07686
Uridine-cytidine kinase 2	UCK2	Q9BZX2
Hexokinase-1	HK1	P19367
Heat shock protein HSP 90-alpha	HSP90AA1	P07900
histone mRNA exonuclease 1	ERI1	Q8IV48
Protein-glutamine gamma-glutamyltransferase E	TGM3	Q08188
Deoxycytidine kinase	DCK	P27707
Methionine aminopeptidase 2	METAP2	P50579
Proto-oncogene tyrosine-protein kinase LCK	LCK	P06239
Leukocyte elastase	ELANE	P08246
Ephrin type-A receptor 2	EPHA2	P29317
Cathepsin K	CTSK	P43235
Nitric oxide synthase, inducible	NOS2	P35228
Death-associated protein kinase 1	DAPK1	P53355
Prothrombin	F2	P00734
Hypoxanthine-guanine phosphoribosyltransferase	HPRT1	P00492
Histo-blood group ABO system transferase	ABO	P16442
Glutathione S-transferase P	GSTP1	P09211
Vitamin D3 receptor	VDR	P11473
E-selectin	SELE	P16581
Lanosterol synthase	LSS	P48449
Tyrosine-protein phosphatase non-receptor type 1	PTPN1	P18031
ADP-ribosylation factor-like protein 5B	ARL5B	Q96KC2
Mitogen-activated protein kinase 10	MAPK10	P53779
Dipeptidase 1	DPEP1	P16444
Estradiol 17-beta-dehydrogenase 1	HSD17B1	P14061
UDP-N-acetylhexosamine pyrophosphorylase	UAP1	Q16222
Sulfotransferase family cytosolic 2B member 1	SULT2B1	O00204
Thymidylate kinase	DTYMK	P23919
Aldo-keto reductase family 1 member C2	AKR1C2	P52895
GTP-binding nuclear protein Ran	RAN	P62826
Riboflavin kinase	RFK	Q969G6
S-methyl-5-thioadenosine phosphorylase	MTAP	Q13126
Mitogen-activated protein kinase 14	MAPK14	Q16539
Beta-secretase 1	BACE1	P56817
3-phosphoinositide-dependent protein kinase 1	PDPK1	O15530
Serine/threonine-protein kinase 6	AURKA	O14965
Chitotriosidase-1	CHIT1	Q13231
Phenylethanolamine N-methyltransferase	PNMT	P11086
Cell division protein kinase 2	CDK2	P24941
Proto-oncogene tyrosine-protein kinase Src	SRC	P12931
Tryptophan 5-hydroxylase 1	TPH1	P17752
Early endosome antigen 1	EEA1	Q15075
5(3)-deoxyribonucleotidase, mitochondrial	NT5M	Q9NPB1
Glucose-6-phosphate isomerase	GPI	P06744
Ras-related protein Rap-2a	RAP2A	P10114
Glycogen phosphorylase, liver form	PYGL	P06737
Apoptotic protease-activating factor 1	APAF1	O14727
Corticosteroid 11-beta-dehydrogenase isozyme 1	HSD11B1	P28845

Androgen receptor	AR	P10275
Glutathione S-transferase Mu 2	GSTM2	P28161
Glutathione S-transferase A3	GSTA3	Q16772
cAMP-specific 3,5-cyclic phosphodiesterase 4D	PDE4D	Q08499
Carbonic anhydrase 2	CA2	P00918
Deoxyuridine 5-triphosphate nucleotidohydrolase, mitochondrial	DUT	P33316
Histamine N-methyltransferase	HNMT	P50135
Renin	REN	P00797
Nuclear factor erythroid 2-related factor 2	NFE2L2	Q16236
Tryptophanyl-tRNA synthetase, cytoplasmic	WARS	P23381
Dual specificity mitogen-activated protein kinase kinase 1	MAP2K1	Q02750
Serum albumin	ALB	P02768
Cyclin-A2	CCNA2	P20248
Neutrophil collagenase	MMP8	P22894
cAMP-dependent protein kinase catalytic subunit alpha	PRKACA	P00517
Glucocorticoid receptor	NR3C1	P04150
ADP-ribosyl cyclase 2	BST1	Q10588
Baculoviral IAP repeat-containing protein 7	BIRC7	Q96CA5
Maleylacetoacetate isomerase	GSTZ1	O43708
Glucosylceramidase	GBA	P04062
Estrogen recepto	ESR1	P03372
Inosine-5-monophosphate dehydrogenase 2	IMPDH2	P12268
Protein S100-A9	S100A9	P06702
Alcohol dehydrogenase class-3	ADH5	P11766
Peptidyl-prolyl cis-trans isomerase FKBP1A	FKBP1A	P62942
tRNA (cytosine-5-)-methyltransferase	TRDMT1	O14717
Histidine triad nucleotide-binding protein 1	HINT1	P49773
Mast/stem cell growth factor recepto	KIT	P10721
Sepiapterin reductase	SPR	P35270
Caspase-1	CASP1	P29466
Ferrochelatase, mitochondrial	FECH	P22830
Tyrosine-protein kinase JAK2	JAK2	O60674
Aldose reductase	AKR1B1	P15121
Thymidylate synthase	TYMS	P04818
Sex hormone-binding globulin	SHBG	P04278
Amine oxidase [flavin-containing] B	MAOB	P27338
Fibrinogen gamma chain	FGG	P02679
Tyrosine-protein kinase HCK	HCK	P08631
Glutathione S-transferase theta-2	GSTT2B	P0CG30
NAD-dependent deacetylase sirtuin-5	SIRT5	Q9NXA8
Glutathione S-transferase A1	GSTA1	P08263
Proto-oncogene serine/threonine-protein kinase Pim-1	PIM1	P11309
Estrogen receptor beta	ESR2	Q92731
Insulin receptor	INSR	P06213
RAC-beta serine/threonine-protein kinase	AKT2	P31751
Serine/threonine-protein phosphatase PP1-gamma catalytic subunit	PPP1CC	P36873
Mitogen-activated protein kinase 1	MAPK1	P28482
Glycogen synthase kinase-3 beta	GSK3B	P49841

Supplementary Table 2. Topological feature values of targets for Lycopene preventing cutaneous tumor.

Candidate targets GENE NAME	DC(>111)	EC(>0.039842676)	LAC(>24.66197183)	BC(>1606.42844)	CC(>0.339340764)	NC(>36.7491238)
ABCC2	187	0.045459241	24.84408602	9005.802877	0.347414421	68.46314328
ABCC4	305	0.094544813	38.28618421	13699.7453	0.35775	130.7524166
ATG12	325	0.093174718	30.97222222	12510.34332	0.358556753	120.1888415
ATG3	170	0.045113869	32.04142012	5216.234315	0.345318533	68.56396477
ATG4	118	0.040851254	26.58974359	1696.036371	0.340309156	39.22334829
ATG5	136	0.047911584	24.88888889	3248.988206	0.342344498	38.8965772
BCL2	216	0.069759451	31.7627907	4482.16925	0.348005837	74.56607043
BECN1	132	0.050224762	28.71755725	2447.53254	0.341201717	38.96404899
BRCA1	229	0.061842397	29.9122807	9281.742982	0.350649351	83.11698941
CAND1	257	0.088335834	44.3671875	5848.056945	0.351856405	121.112482
CAT	297	0.095324956	42.10472973	9978.227127	0.356058721	134.0250891
UGT1A6	401	0.101440765	31.1675	34118.21889	0.365984655	171.5034149
CUL3	407	0.115885355	40.88423645	24462.79402	0.367017184	197.2527924
CYP1A1	205	0.06863936	29.61764706	4398.16936	0.34657302	66.2786147
E2F1	338	0.099740505	34.33234421	18813.26649	0.359909457	134.140268
CES1R	289	0.061022762	25.23958333	22322.9337	0.35667996	113.2022051
TNFSF15	341	0.090039417	34.64705882	25872.36959	0.361363636	153.0423094
GABARAP	140	0.058590103	35.47482014	1898.237411	0.342754491	48.34950655
GCLC	147	0.0477276	34.95205479	2191.891671	0.341935484	58.74549889
GCLM	142	0.051684093	31.26950355	1895.099055	0.341527446	49.3583818
GPX1	183	0.065052092	33.65934066	3556.437636	0.34457019	64.67704418
GRB2	241	0.058540106	25.25	17419.63786	0.352116142	89.14903859
GSTA2	142	0.056025203	34.65957447	1951.962231	0.341772152	51.10983269
GSTM3	210	0.063890435	27.15789474	5601.380232	0.347414421	65.22987287
GSTT1	174	0.063643008	36.75722543	4759.911411	0.345735685	64.08725927
HDAC1	198	0.05421263	35.39593909	6851.173308	0.348090489	88.68155071
HMOX1	226	0.05821839	34.08888889	9092.883339	0.350735294	96.94870092
HNRNPM	141	0.056462422	39.79432624	1662.939308	0.341772152	58.86623363
HNRNPU	174	0.065748565	38.20114943	3281.265977	0.345401883	69.09646809
HSP90AA1	339	0.082687452	33.62426036	31931.63971	0.361546235	164.7935414
HSP90AB1	267	0.070742942	29.7406015	17922.35124	0.35464684	109.7798907
HSPA1A	132	0.048693269	27.44274809	1864.405051	0.342017208	40.24812122
HSPA1B	132	0.048693269	27.44274809	1864.405051	0.342017208	40.24812122
HSPA5	160	0.058036871	29.9	3468.738646	0.344819277	50.6036435
HSPA8	180	0.062471829	32.83240223	5918.755949	0.346825012	59.95911373
ILF3	137	0.056275345	40.18978102	2331.045394	0.341039085	55.95388237
ITGA4	270	0.083415017	31.17472119	7562.414094	0.35368265	92.31751939
KEAP1	128	0.048658811	26.13385827	3073.985256	0.340309156	37.50242308
MAPK14	187	0.051795304	25.40322581	6723.270842	0.346825012	59.11954833
MAPK8	136	0.042939164	25.40740741	2383.545205	0.341364504	37.29512941
RXRA	224	0.058828417	24.86995516	8653.855305	0.350735294	69.8637354
NEDD8	303	0.093732998	39.20198675	12086.99334	0.357214179	130.9642558
NPM1	204	0.076828629	43.01477833	4349.055097	0.348599269	80.91094074
NQO1	171	0.064798295	36.90588235	2511.443348	0.345401883	63.25168001
OBSL1	274	0.080773741	28.08791209	7788.298099	0.353420598	92.19721579

PAN2	177	0.06097826	26.20454545	2525.552876	0.343659942	49.2803812
PARP1	157	0.054239359	32.69230769	3737.515667	0.344238634	54.62459615
PIK3C3	144	0.047793798	25.74125874	2406.579138	0.342754491	40.70780914
PRKDC	149	0.05278014	27.99324324	3848.36108	0.344155844	44.66920169
RNF2	261	0.07375174	29.17307692	9571.492768	0.352463054	92.0338035
RPA1	168	0.055030849	28.65868263	3530.430959	0.344238634	54.14086487
RPS27A	149	0.04911413	30.58108108	3400.264724	0.342754491	52.10114428
SLC2A5	123	0.044492684	26.1147541	1714.945766	0.339501779	38.54230868
SLC6A15	256	0.080202766	28.19215686	5862.321258	0.351942941	79.89887905
SMARCA4	132	0.042924434	31.64885496	2428.652733	0.340552118	50.2666139
SOD2	526	0.129363835	38.59047619	55258.12593	0.378471304	274.9394148
SQSTM1	132	0.047083173	25.96183206	2480.463799	0.341853798	39.09137158
STAU1	168	0.05662981	27.60479042	2627.715126	0.343659942	50.88887432
SUMO1	354	0.096740618	35.40509915	21643.43319	0.361911988	150.7748874
SUMO3	325	0.096635871	35.95061728	15656.75364	0.358466934	134.749212
SUZ12	166	0.048357066	25.02424242	3604.252635	0.342918763	48.82167063
TARDBP	161	0.058899906	37.3	2500.246986	0.343083193	64.12700197
TP53	389	0.105065025	40.52835052	31882.01865	0.365797546	190.5462544
TUBB	131	0.049730685	26.50381679	1763.81893	0.342098972	37.64882082
TXNRD1	339	0.102408722	43.83727811	20720.81764	0.361454913	164.0209297
UBC	1310	0.239188775	56.85026738	795175.8572	0.479557641	1310.861462
UBL4A	139	0.048587617	30.18115942	1804.806801	0.340471092	46.31340527
UGT1A1	176	0.0592997	33.22857143	4093.978998	0.345485273	62.79719772
ULK1	197	0.062763587	31.25510204	5685.021811	0.347667638	68.03153982
VCP	213	0.065383755	31.54716981	8173.289899	0.349621305	76.80972806
YWHAG	173	0.051689923	27.61046512	4841.588854	0.345902828	58.95030038